Frontiers in Heat and Mass Transfer (FHMT), 12, 3 (2019)
DOI: 10.5098/hmt.12.3

Global Digital Central
ISSN: 2151-8629

Frontiers in Heat and Mass Transfer

Available at www.ThermalFluidsCentral.org

MAGNETO-CONVECTION OF ALUMINA - WATER NANOFLUID WITHIN THIN HORIZONTAL LAYERS USING THE REVISED GENERALIZED BUONGIORNO'S MODEL

A.Wakif [a,*], Z. Boulahia[a], A. Amine[b], I.L. Animasaun[c], M. I. Afridi[d], M. Qasim[d], R. Sehaqui[a]

[a]*Hassan II University, Faculty of Sciences Aïn Chock, Laboratory of Mechanics, B.P.5366 Mâarif, 20100 Casablanca, Morocco.*
[b]*Hassan II University, Faculty of Sciences and Technology, Laboratory of Condensed Matter and Renewable Energy, Mohammedia, Morocco.*
[c]*Department of Mathematical Sciences, Federal University of Technology, Akure, Nigeria.*
[d]*Department of Mathematics, COMSATS University Islamabad (CUI), Park Road, Tarlai Kalan, Islamabad-455000, Pakistan.*

ABSTRACT

The significance of an externally applied magnetic field and an imposed negative temperature gradient on the onset of natural convection in a thin horizontal layer of alumina-water nanofluid for various sizes of spherical alumina nanoparticles (e.g., $30nm$, $35nm$, $40nm$, $45nm$) and volumetric fractions (e.g., 0.01, 0.02, 0.03, 0.04) is explored and analyzed numerically in this paper. The generalized Buongiorno's mathematical model with the simplified Maxwell's equations and the Oberbeck-Boussinesq approximation were adopted to simulate the two-phase transport phenomena, in which the Brownian motion and thermophoresis aspects are taken into account. Moreover, the rheological behavior of alumina-water nanofluid and related flow are assumed to be Newtonian, incompressible and laminar. Based on the linear stability theory, the perturbed partial differential equations (PDEs) of magnetohydrodynamic convective nanofluid flow are firstly simplified formally using the normal mode analysis technique and secondly converted to a generalized eigenvalue problem considering more realistic boundary conditions, in which the thermal Rayleigh number is the associated eigenvalue. Additionally, the resulting eigenvalue problem was solved numerically using powerful collocation methods, like Chebyshev-Gauss-Lobatto Spectral Method (CGLSM) and Generalized Differential Quadrature Method (GDQM). Furthermore, the thermo-magneto-hydrodynamic stability of the nanofluidic system and the critical size of convection cells are highlighted graphically in terms of the critical thermal Rayleigh and wave numbers, for various values of the magnetic Chandrasekhar number, the volumetric fraction and the diameter of alumina nanoparticles.

Keywords: *Linear Stability Analysis; Nanofluid; Alumina Nanoparticles; Magneto-Convection; Buongiorno's Model; Collocation Methods.*

1. INTRODUCTION

In recent decades, numerous investigations have been conducted on the conventional fluids, in an attempt to enhance their intrinsic thermo-physical properties and consequently improve heating and cooling systems by dispersing insoluble nano-sized particles (Maxwell, 1873) like copper, silver, gold, alumina, copper oxide, titanium dioxide, carbon nanotubes, graphene, graphene oxide and diamond into a specified fluid such as water, ethylene glycol and oil. This new type of working fluids, which was first invented by Choi (1995) is called nanofluids. In other words, the terminology of nanofluid or nanoliquid was introduced scientifically in fluid mechanics and rheology to refer to the fluids with suspended solid nanoparticles of average size less than $100\ nm$. Moreover, these engineered colloidal suspensions of nanoparticles in a chosen base fluid can be synthesized under some experimental conditions to obtain stable homogeneous mixtures. Today, these new innovative materials become among the most commonly used smart fluids, which have gained the significant attention of researchers around the globe, because of their widespread applications in modern science, engineering and industry. After the pioneering theoretical work of Buongiorno (2006), other experimental studies (Buongiorno, 2009 ; Żyła et al., 2018), as well as numerical modeling investigations (Boulahia et al., 2017a, 2017b , 2017c , 2017d) have been carried out by many researchers, in order to show the excellent heat transfer performance of nanofluids and their higher energy storage capacity compared to the commonly used conventional thermal fluids. As the main result, it was found that the inclusion of a small volumetric fraction of nanoparticles inside a base fluid can increase the thermal conductivity of the mixture dramatically, and also improve its thermal performance enormously. All these thermal benefits have made the nanofluids potentially useful in many engineering applications, such as heat and mass transfer enhancement, energy efficient buildings, solar collectors, biomedical applications and many others. Due to the considerable advancement in modern technology and growing demands in the development of efficient and powerful cooling systems, the nanofluid technology has gained worldwide acceptance from researchers in recent years, mainly in the field of cooling systems like nuclear power reactors, transformer oils, devices in automotive vehicles and microelectronic components. Following the same trends, Makinde and Animasaun (2016a , 2016b), Pandey and Kumar (2016 , 2017a , 2017b , 2017c) , Boulahia et al. (2016 , 2018) and Koriko et al. (2018) studied the convection heat transfer behavior of nanofluids and the significance of quartic chemical reactions through various practical engineering problems , in order to achieve a profound understanding of the importance of these liquid substances (i.e., nanofluids or nanoliquids)

* *Corresponding author. Email: wakif.abderrahim@gmail.com*

Global Digital Central
ISSN: 2151-8629

towards the advanced industrial and technological systems requiring ultra-high rates of heating or cooling.

From the chemical and physical point of views, the nanofluids can be actually synthesized in the scientific laboratories by utilizing various experimental methods. In spite of these numerous approaches, there are only two primary ways, namely single-step and two-step processes among the most widely used methods for preparing homogeneous mixtures with almost negligible agglomeration of nanoparticles. These techniques have been carried out by respecting specified experimental protocols, which require careful steps to ensure that the mixture (e.g., base fluid + nanoparticles) remains stable over a long period of time. In addition, the single-step and two-step methods have been classified according to the number of steps involved during their preparation. In the first method, the nanoparticles are prepared and dispersed simultaneously into a base fluid during the manufacturing process of nanoparticles. While in the two-step method, the nanoparticles are first produced either by physical or chemical processes, which can be thereafter dispersed into the base fluid using an intensive magnetic force agitation. In term of the economic cost, the two-step procedure is considered as the easiest method applied by the experimenters to manufacture enhanced working fluids in large and applicable scales. Regardless of the method employed for preparing nanofluids, the nanoparticles always have a tendency to agglomerate or aggregate due to the van der Waals forces. Consequently, the heavier nanoparticles tend to settle at the bottom under the impact of gravitational forces. Due to this fact, many undesirable phase instabilities driven by the agglomeration and sedimentation of nanoparticles can be induced in the medium. For this purpose, it is recommended to introduce suitable surfactants into the nanofluidic medium for suppressing these instabilities. In addition, the presence of surfactant molecules inside the nanofluid can significantly increase the repulsive forces between the nanoparticles. Physically, it is well known that when the repulsive forces are higher than the attractive van der Waals forces, the impact of the agglomeration can be quantitatively reduced for the nanoparticles.

In the light of the aforementioned results, Angayarkanni and Philip (2015) reported in their innovative work that to ensure the stability maintenance of nanofluids, it is suggested to minimize the destabilizing effect of the attractive van der Waals forces either by decreasing the size of solid nanoparticles d_{np}, increasing the base fluid viscosity μ_{bf} or decreasing the density difference between the nanoparticles and the base fluid. Furthermore, it is also proved that due to the presence of the nanoparticles migration inside the base fluids, the nanofluids can achieve a substantial enhancement in the thermal transfer performances. In view of all these results, Wakif et al. (2018a) revealed that the heterogeneity of nanoparticles concentration increases locally with the temperature. The main reasons behind the non-homogeneity in the volumetric fraction of nanoparticles are the Brownian motion and thermophoresis slip mechanisms, which are evidently due to the random movements of nanoparticles and their very small dimensions. In this framework, Buongiorno (2006) in his seminal work suggested a two-component four-equation non-homogeneous equilibrium model for mass, momentum, volumetric fraction of nanoparticles and heat transfer in nanofluids by taking into account the effects of the thermophoresis phenomenon (i.e., movement of solid nanoparticles from the warmer regions to the colder regions) and Brownian motion (i.e., movement of solid nanoparticles from the greater concentration areas to those with lower concentration) as possible slip mechanisms between the base fluid and nanoparticles. In related works, Nield and Kuznetsov (2014a , 2014b) extended the validity of the Buongiorno's mathematical model for the impermeable boundaries, in which the volumetric fraction of solid nanoparticles can be passively rather than actively controlled at the boundaries. In this revised model, the nanoparticles on the impermeable walls are indirectly adjusted via the volumetric fraction gradient of nanoparticles by adopting the condition of zero nanoparticles mass flux. Physically, this newly suggested assumption for controlling the nanoparticles is more realistic as compared to other models. Likewise, this approach remains possible for the nanofluids, as long as the boundaries are assumed impermeable to the base fluid and nanoparticles. Very recently, Animasaun (2016) investigated the dynamics of water conveying alumina nanoparticles on an upper horizontal surface of paraboloid of revolution coated with three molecules of catalyst using quartic autocatalysis chemical reaction. It was observed that the horizontal velocity and temperature distribution across the flow increase with the volumetric fraction of nanoparticles. In another related study about the influence of Hall effect on the flow of $36nm$ alumina-water and $47nm$ alumina-water nanofluids, Animasaun et al. (2018) remarked that the maximum cross-flow velocity is attained within the fluid domain when 36 nm nanoparticles alumina is used.

Nowadays, the Buongiorno's two-phase approach becomes the most plausible and used model for predicting the heat transfer enhancement and analyzing the nanoparticles transportation in nanofluids, owing to its reasonable explanation. Therefore, many researchers are constantly working to develop this heterogeneous model, in order to improve its capability as an advanced mathematical model for simulating the two-phase convective flows (i.e., natural, forced or mixed convection flows) and estimating the heat transfer performance of nanofluids. Lately, this model has been generalized to take care of the nanofluid flow variables, due to the effective dependence of the thermophysical properties of nanofluids on the temperature and the volume fraction of nanoparticles. Based on the revised form of the Buongiorno's two-phase model, several interesting investigations were reported by many researchers using the generalized version of the heterogeneous two-phase model. Among the more recent researches on nanofluids, it can be found a lot of related papers in the literature survey regarding the generalized Buongiorno's nanofluid model. To mention a few, Garoosi and Talebi (2017) used the Buongiorno's two - phase model to examine a numerical simulation of the combined conduction and natural convection nanofluid flows and temperature distribution in an enclosure with the presence of vertical partition or several conductive obstacles with finite thickness and thermal conductivity. In this regard, the authors used Corcione's correlations (Corcione, 2011) as the best ways for estimating the effective thermal conductivity k_{nf} and dynamic viscosity μ_{nf}. Alsabery et al. (2018) investigated the problem of conjugate natural convection of Al_2O_3 - water nanofluids in a square cavity with concentric solid insert and isothermal corner boundaries using the non-homogenous Buongiorno's two-phase model in combination with the Corcione's correlations. Astanina et al. (2018) adopted the heterogeneous Buongiorno's model to investigate the natural convection in a partially heated enclosure by considering the dependence of thermophysical properties of CuO- water nanofluids on temperature T^* and volume fraction ϕ^*. Accordingly, the researchers who authored this work recommended employing Chon's correlation (Chon et al., 2005) for predicting the effective thermal conductivity k_{nf} and another powerful model developed by Nguyen et al. (2007) to estimate the effective dynamic viscosity μ_{nf} based on experimental data.

Owing to the relevance of heat transfer of nanofluids and their widespread usage area in today's advanced nanotechnologies, other related investigations on SiO_2 - ethylene glycol nanofluids have been carried out experimentally by Żyła and Fal (2017) to measure the effective dynamic viscosity μ_{nf} and thermal conductivity k_{nf} as well as the electrical conductivity σ_{nf}. This great work has been subsequently extended and analyzed by Żyła et al. (2018) in the same manner for ethylene glycol (EG) - based nanofluids containing nanodiamonds (ND), in order to explore the rheological, thermophysical and dielectric properties of these nanofluids. Among the main results of these experimental investigations, it was found that the thermal conductivity k_{nf} and the electrical conductivity σ_{nf} of SiO_2 - ethylene glycol and ND - ethylene glycol nanofluids generally increase with the volumetric fraction of solid nanoparticles ϕ_0 according to the specified empirical correlations. Similarly, it was furtherly reported that the electrical conductivity σ_{nf} can be increased with the inclusion of some typical

Global Digital Central
ISSN: 2151-8629

nanoparticles within a specified base fluid. For instance, Naddaf and Heris, (2018) measured the electrical conductivity σ_{nf} of diesel oil (DO)- based nanofluids containing graphene nanoplatelets (GNP) or multi-walled carbon nanotubes $(MWCNT)$ as solid nanoparticles and hexylamine (HA) or oleic acid (OA) as suitable surfactants. In this investigation, the electrical conductivity was greatly improved with the increase in nanomaterials concentration and temperature. This stems from the fact that the interaction between the nanoparticles is increased with the concentration as well as the electrons of the solid phase can be thermally excited from the valence band to the conduction band for enhancing the electrical conductance of the mixture and producing the so-called electrically conducting nanofluid, whose the flow behavior can be influenced by the existence of Lorentz forces generated within the medium under the effect of an externally applied magnetic field.

Over the last several decades, a wide variety of practical engineering problems dealing with the magnetohydrodynamic (MHD) convective heat and mass transfer flows have attracted substantial attention by many researchers, due to their widespread and vital potential applications in technological and industrial disciplines. More recently, tremendous research works focusing on the magnetohydrodynamic convective flows of electrically conducting fluids or nanofluids were reported previously by many researchers. Later, Amanulla et al. (2018) performed a thorough numerical investigation to simulate the steady MHD convective flow of Carreau non-Newtonian fluid past an isothermal sphere by applying Keller-Box Method (KBM). Qasim et al. (2018) conducted an innovative numerical simulation of MHD peristaltic flow with variable electrical conductivity and joule dissipation by utilizing Generalized Differential Quadrature Method (GDQM). On the other hand, a comprehensive survey was done by Wakif et al. (2017a) on the thermo-magneto-hydrodynamic stability of nanofluids saturating porous mediums by means of Chebyshev-Gauss-Lobatto Spectral Method (CGLSM). Similarly, Rana et al. (2017) studied the onset of thermo-magneto-hydrodynamic instability in a rotating viscoelastic nanofluid layer under the influence of an internal heat source with the help of Galerkin Weighted Residuals Technique (GWRT). Also, Akbarzadeh (2018) carried out a numerical study concerning the effect of a purely internal heat generation and chemical reaction on the onset of thermo-magneto-hydrodynamic instabilities inside a porous medium saturated by a nanofluid by using GWRT. In another stability problem, Wakif et al. (2018b) proposed a generalized mathematical formulation to perform numerical examinations of the thermo-magneto-hydrodynamic stability of some metallic nanofluids by considering the Buongiorno's and Corcione's models and utilizing Runge-Kutta-Fehlberg Method (RKFM) as a powerful approach for implementing the stability problems.

Based on the above-cited papers concerning the thermo-magneto-hydrodynamic stability of nanofluids, it is found that there is a great lack of numerical works dealing with the realistic analysis of the thermo-magneto-hydrodynamic instabilities occurred inside the electrically conducting nanofluids under the effects of buoyancy and Lorentz forces. However, to the best of author's knowledge, the revised form of the generalized Buongiorno's two-phase model with the assumption of zero nanoparticles mass flux condition has not been given any attention from researchers, despite the importance of magneto-convection in many thermal engineering systems. Inspired by the above-mentioned works, our configuration of interest focuses on using the revised Buongiorno's mathematical model as a more realistic approach for analyzing the thermo-magneto-hydrodynamic stability of alumina-water nanofluids by considering the Chon's and Corcione's nanofluid models for estimating the effective thermal conductivity k_{nf} and dynamic viscosity μ_{nf}, respectively. Likewise, the resulting stability equations are solved numerically with a good accuracy by utilizing Chebyshev-Gauss-Lobatto Spectral Method (CGLSM) and Generalized Differential Quadrature Method (GDQM), for non-slip, impermeable, zero nanoparticles mass flux and isothermal boundary conditions. Moreover, the present findings are multiply validated by comparing our numerical outcomes with the results of the existing literature. Furthermore, the effects of various emerging parameters $(\text{i.e.}, Q, \phi_0 \text{ and } d_{np})$ on the criterion for the onset of magneto-convection in alumina-water nanofluids are provided in the form of graphical and tabular illustrations coupled with comprehensive discussions.

2. PROBLEM FORMULATION

The schematic diagram of the studied problem is depicted in Fig. 1. In this physical configuration, we consider a thin horizontal layer of a dilute colloidal suspension containing spherical alumina nanoparticles Al_2O_3 dispersed into a pure water H_2O. A fixed spatial Cartesian frame of reference (x^*, y^*, z^*) is located in the lower level of the plates (IHP) and (ICP), in which the z^*-axis is directed vertically upwards. Also, the studied homogeneous mixture $(Al_2O_3 + H_2O)$ is assumed electrically conducting nanofluid, incompressible fluid, has Newtonian rheological behavior, confined between two electrically non-conducting infinite parallel plates, subjected to a uniform gravitational field $\mathbf{g}$, heated from below and affected by an external transverse magnetic field $\mathbf{H_0}$ with a constant magnetic strength H_0. In order to simplify the proposed model, the viscous dissipation, Ohmic heating and Hall effects are not taken into account in the present numerical examination. As imposed boundary conditions, the lower and upper boundaries are maintained at constant temperatures T_h and T_c $(T_c < T_h)$, respectively, whereas the volumetric fraction of solid nanoparticles is controlled passively at the horizontal impermeable plates, in such a way that the vertical component J_z^* of the nanoparticles mass flux is assumed to be zero on these boundaries $(\text{i.e.}, (\partial\phi^*/\partial z^*) + [D_T/(D_B T_c)]\,(\partial T^*/\partial z^*) = 0)$, in which there are no slip velocities between the nanofluid and the plates (IHP) and (ICP). For a given volumetric fraction of nanoparticles ϕ_0, the thermophysical properties of alumina-water nanofluids (e.g., dynamic viscosity μ_{nf}, thermal conductivity k_{nf}, specific heat c_{nf}, magnetic permeability $\bar{\mu}_{nf}$ and electrical conductivity σ_{nf}) are assumed to remain constant in the vicinity of the cold plate temperature T_c, except for the density ρ in the gravitational force $\mathbf{F_g} = -\rho\, g\, \mathbf{e_z}$, which is estimated formally based on the Oberbeck-Boussinesq approximation.

According to Buongiorno (2006) and Wakif et al. (2017b , 2018b), the various partial differential equations governing the nanofluid flow, heat and mass transfer in the presence of an external magnetic field are written as follows:

$$\nabla^*.\mathbf{V}^* = 0 \tag{1}$$

$$\rho_{nf}\left[\frac{\partial \mathbf{V}^*}{\partial t^*} + (\mathbf{V}^*.\nabla^*)\mathbf{V}^*\right] = -\nabla^* P^* + \mu_{nf}\,\nabla^{*2}\mathbf{V}^* + \mathbf{F_g} + \mathbf{F_m} \tag{2}$$

$$\frac{\partial T^*}{\partial t^*} + (\mathbf{V}^*.\nabla^*)T^* = \frac{k_{nf}}{(\rho c)_{nf}}\nabla^{*2}T^* + \frac{(\rho c)_{np}}{(\rho c)_{nf}}\left[\begin{matrix} D_B\nabla^*\phi^*.\nabla^*T^* \\ +\dfrac{D_T}{T_c}\nabla^*T^*.\nabla^*T^* \end{matrix}\right] \tag{3}$$

$$\frac{\partial \phi^*}{\partial t^*} + (\mathbf{V}^*.\nabla^*)\phi^* = D_B\nabla^{*2}\phi^* + \frac{D_T}{T_c}\nabla^{*2}T^* \tag{4}$$

$$\frac{\partial \mathbf{H}^*}{\partial t^*} + (\mathbf{V}^*.\nabla^*)\mathbf{H}^* = (\mathbf{H}^*.\nabla^*)\mathbf{V}^* + \eta_{nf}\,\nabla^{*2}\mathbf{H}^* \tag{5}$$

$$\nabla^*.\mathbf{H}^* = 0 \tag{6}$$

Within the framework of the above-mentioned assumptions, the gravitational body force $\mathbf{F_g}$ (Wakif et al., 2018a , 2018b, 2018c) and the Lorentz force $\mathbf{F_m}$ (Chandrasekhar, 1961) are expressed by:

$$\mathbf{F_g} = -\left[1 - \beta_{nf}\,(T^* - T_c) + \beta_\phi\,(\phi^* - \phi_0)\right]\rho_{nf} g\,\mathbf{e_z} \tag{7}$$

$$\mathbf{F_m} = \frac{\bar{\mu}_{nf}}{4\pi}(\nabla^* \times \mathbf{H}^*) \times \mathbf{H}^* \tag{8}$$

Global Digital Central
ISSN: 2151-8629

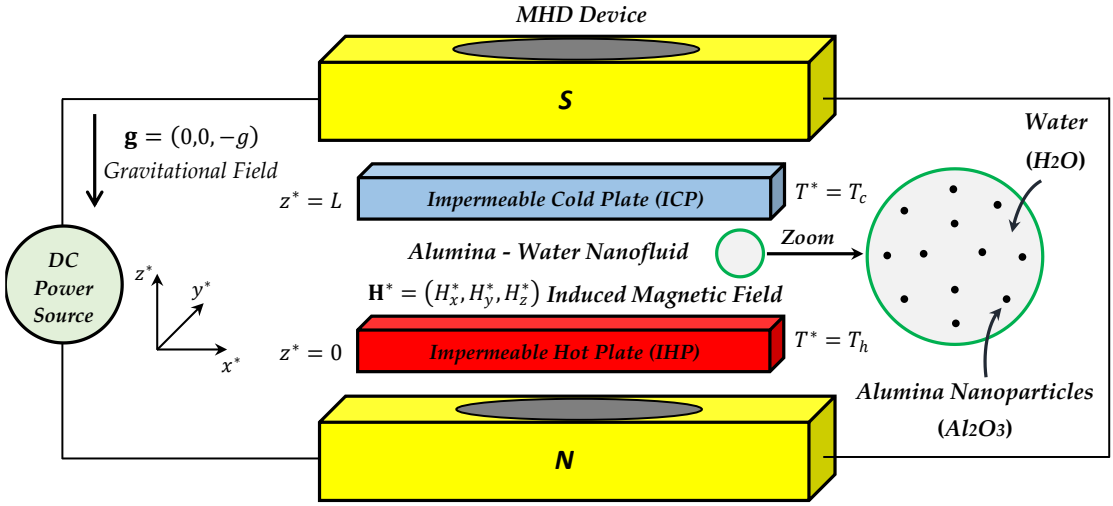

Fig. 1 Description of the physical flow model.

Here, $\mathbf{V}^*$ is the nanofluid velocity vector, $\mathbf{H}^*$ denotes the induced magnetic field and ∇^* refers to the nabla vector operator, whereas t^*, P^*, T^*, ϕ^* represent the time, the pressure, the temperature and the volume fraction of solid nanoparticles, respectively, where $\mathbf{V}^* = (u^*, v^*, w^*)$, $\mathbf{H}^* = (H_x^*, H_y^*, H_z^*)$ and $\nabla^* = (\partial/\partial x^*, \partial/\partial y^*, \partial/\partial z^*)$.

Following Buongiorno (2006), McNab and Meisen (1973), the Brownian diffusion coefficient D_B and the thermophoretic diffusion coefficient D_T shown in Eqs. (3) and (4) can be calculated at the reference state $(\text{i.e.}, (T^*, \phi^*) = (T_c, \phi_0))$ by:

$$D_B = \frac{k_B T_c}{3\pi\, \mu_{bf}\, d_{np}} \tag{9}$$

$$D_T = 0.26\left(\frac{k_{bf}}{2k_{bf} + k_{np}}\right)\left(\frac{\mu_{bf}}{\rho_{bf}}\right)\phi_0 \tag{10}$$

In addition, the physical problem under consideration is subjected to the following boundary conditions:

$$w^* = \frac{\partial w^*}{\partial z^*} = 0\,,\; T^* = T_h\,, \frac{\partial \phi^*}{\partial z^*} + \frac{D_T}{D_B T_c}\frac{\partial T^*}{\partial z^*} = 0 \;\text{ at }\; z^* = 0 \tag{11}$$

$$w^* = \frac{\partial w^*}{\partial z^*} = 0\,,\; T^* = T_c\,, \frac{\partial \phi^*}{\partial z^*} + \frac{D_T}{D_B T_c}\frac{\partial T^*}{\partial z^*} = 0 \;\text{ at }\; z^* = L \tag{12}$$

As is well-known, the nanofluid properties depend strongly on the values of temperature and volumetric fraction of nanoparticles taken into account during the estimation. Accordingly, the effective thermo-physical properties of Alumina - water nanofluids like the density ρ_{nf}, the thermal diffusivity α_{nf}, the specific heat capacity $(\rho c)_{nf}$, the volumetric mass expansion coefficient $(\rho\beta)_{nf}$, the electrical conductivity σ_{nf}, the magnetic permeability $\bar{\mu}_{nf}$ and the magnetic diffusivity η_{nf} are given by Garnett (1905), Sihvola and Lindell (1992) and Wakif et al. (2018a, 2018b) as follows:

$$\rho_{nf} = (1-\phi_0)\,\rho_{bf} + \phi_0\,\rho_{np} \tag{13}$$

$$\alpha_{nf} = \frac{k_{nf}}{(\rho c)_{nf}} \tag{14}$$

$$(\rho c)_{nf} = (1-\phi_0)(\rho c)_{bf} + \phi_0\,(\rho c)_{np} \tag{15}$$

$$(\rho\beta)_{nf} = (1-\phi_0)(\rho\beta)_{bf} + \phi_0\,(\rho\beta)_{np} \tag{16}$$

$$\frac{\sigma_{nf}}{\sigma_{bf}} = 1 + \frac{3\left[\left(\sigma_{np}/\sigma_{bf}\right) - 1\right]\phi_0}{\left[\left(\sigma_{np}/\sigma_{bf}\right) + 2\right] - \left[\left(\sigma_{np}/\sigma_{bf}\right) - 1\right]\phi_0} \tag{17}$$

$$\frac{\bar{\mu}_{nf}}{\bar{\mu}_{bf}} = 1 + \frac{3\left[\left(\bar{\mu}_{np}/\bar{\mu}_{bf}\right) - 1\right]\phi_0}{\left[\left(\bar{\mu}_{np}/\bar{\mu}_{bf}\right) + 2\right] - \left[\left(\bar{\mu}_{np}/\bar{\mu}_{bf}\right) - 1\right]\phi_0} \tag{18}$$

$$\eta_{nf} = \frac{1}{4\pi\,\bar{\mu}_{nf}\,\sigma_{nf}} \tag{19}$$

Here, the subscripts nf, np and bf represents the nanofluid, the solid nanoparticles and the base fluid, respectively.

Furthermore, the magnetic permeabilities of alumina $\bar{\mu}_{np}$ and water $\bar{\mu}_{bf}$ can be concluded from their corresponding magnetic susceptibilities χ_{np} and χ_{bf}, respectively, using the following formulas:

$$\bar{\mu}_{np} = \bar{\mu}_0(1 + \chi_{np}) \tag{20}$$

$$\bar{\mu}_{bf} = \bar{\mu}_0(1 + \chi_{bf}) \tag{21}$$

Here, $\bar{\mu}_0$ represents the magnetic permeability of free space, where $\bar{\mu}_0 = 4\pi \times 10^{-7}\; H\; m^{-1}$. In order to perform a realistic prediction of the other effective thermophysical properties of Al_2O_3 - water nanofluids, the effective thermal conductivity k_{nf} and dynamic viscosity μ_{nf} can be computed efficiently at the reference state by making use of Chon's and Corcione's nanofluid models, respectively, which are expressed by :

$$\frac{k_{nf}}{k_{bf}} = 1 + 64.7\phi_0^{0.746}\left(\frac{d_{bf}}{d_{np}}\right)^{0.369}\left(\frac{k_{np}}{k_{bf}}\right)^{0.7476} Pr^{\,0.9955} Re^{\,1.2321} \tag{22}$$

$$\frac{\mu_{nf}}{\mu_{bf}} = \frac{1}{1 - 34.87\left(d_{np}/d_{bf}\right)^{-0.3}\phi_0^{1.03}} \tag{23}$$

The Reynolds number R_e and the molecular diameter of water d_{bf} shown above can be computed from:

$$R_e = \frac{\rho_{bf}\, k_B T_c}{3\pi\, \mu_{bf}{}^2\, l_{bf}} \tag{24}$$

$$d_{bf} = 0.1\left(\frac{6M}{N_{av}\pi\,\rho_{f0}}\right)^{\frac{1}{3}} \tag{25}$$

Here, k_B represents the Boltzmann constant, l_{bf} denotes the mean-free path for water and d_{np} refers to the diameter of alumina nanoparticles Al_2O_3, whereas M, N_{av} and ρ_{f0} show the molecular mass weight of water, the Avogadro number and the density of water at $293K$, respectively, where $k_B = 1.38066 \times 10^{-23} JK^{-1}$, $l_{bf} = 0.17nm$, $M = 18\; g\; mol^{-1}$, $N_{av} = 6.022 \times 10^{23}\; mol^{-1}$ and $\rho_{f0} = 998\; kg\; m^{-3}$.

Global Digital Central
ISSN: 2151-8629

Consequently, by virtue of Eqs. (13) - (25) , the thermophysical properties ρ_{nf} , α_{nf} , $(\rho c)_{nf}$, $(\rho\beta)_{nf}$, σ_{nf} , $\bar{\mu}_{nf}$, η_{nf} , k_{nf} and μ_{nf} of Al_2O_3 - water nanofluids can be computed realistically based on the thermophysical properties of alumina nanoparticles Al_2O_3 and pure water H_2O given by Schenck (1996) and Mehmood et al. (2017) at $T_c = 300\,K$ as shown in Table 1.

Table 1 Thermophysical properties of water and alumina nanoparticles.

Properties	Pure Water	Alumina Nanoparticles
	H_2O	Al_2O_3
$d\ (\times 10^{-9}\,m)$	0.385	30 - 45
$\rho\ (kg\,m^{-3})$	997.1	3970
$c\ (J\,kg^{-1}\,K^{-1})$	4179	765
$k\ (W\,m^{-1}\,K^{-1})$	0.613	40
$\beta\ (\times 10^{-5}\,K^{-1})$	21	0.85
$\sigma\ (S\,m^{-1})$	0.05	10^{-10}
$\chi\ (\times 10^{-6})$	-9.05	-18.1
$\mu\ (\times 10^{-5}\,Pa\,s)$	89	----------

In order to reformulate the present physical problem in another way, the governing partial differential equations can be written in non-dimensional form by introducing the following dimensionless variables:

$$(x\,,y\,,z) = (x^*,y^*,z^*)/L\ ,\ t\ =\ \left(\alpha_{bf}/L^2\right)t^*\ ,$$
$$P\ =\left[L^2/\left(\rho_{bf}\ \alpha_{bf}^2\right)\right]P^*\ ,\ \mathrm{T}\ =(T^*-T_c)/\Delta T\ , \tag{26}$$
$$\phi = (\phi^*-\phi_0)/\phi_0\ ,\ \ \mathbf{V} = \left(L/\alpha_{bf}\right)\mathbf{V}^*\ ,\ \ \mathbf{H} = \mathbf{H}^*/H_0\ .$$

Then, after making use of the non-dimensionalization procedure, Eqs. (1) - (6) reduce to:

$$\nabla.\mathbf{V} = 0 \tag{27}$$

$$\frac{\partial \mathbf{V}}{\partial \mathrm{t}} + (\mathbf{V}.\nabla)\mathbf{V} = -\frac{1}{f_\rho}\nabla p + f_1\nabla^2\,\mathbf{V} + \begin{bmatrix}(f_2R_aT - f_3\phi)\mathbf{e_z}\\ +f_4(\nabla\times\mathbf{H})\times\mathbf{H}\end{bmatrix} \tag{28}$$

$$\frac{\partial T}{\partial t} + (\mathbf{V}.\nabla)T = f_5\nabla^2T + f_6\nabla\phi\,.\nabla T + f_7\,\nabla T\,.\nabla T \tag{29}$$

$$\frac{\partial \phi}{\partial t} + (\mathbf{V}.\nabla)\phi = f_8\,\nabla^2\phi + f_9\,\nabla^2T \tag{30}$$

$$\frac{\partial \mathbf{H}}{\partial t} + (\mathbf{V}.\nabla)\mathbf{H} = (\mathbf{H}\,.\nabla)\mathbf{V} + f_{10}\,\nabla^2\mathbf{H} \tag{31}$$

$$\nabla.\mathbf{H} = 0 \tag{32}$$

Here, the modified dimensionless pressure p shown in Eq. (28) is given by $p = P + f_\rho P_r R_a z/\left(\beta_{bf}\Delta T\right)$, where $\Delta T = T_h - T_c$.

In view of Eq. (26), the boundary conditions (11) and (12) become:

$$w = \frac{\partial w}{\partial z} = 0\,,T = 1\,,\frac{\partial \phi}{\partial z} = -\left(\frac{N_t}{N_b}\right)\frac{\partial T}{\partial z}\quad \text{at}\quad z = 0 \tag{33}$$

$$w = \frac{\partial w}{\partial z} = 0\,,T = 0\,,\frac{\partial \phi}{\partial z} = -\left(\frac{N_t}{N_b}\right)\frac{\partial T}{\partial z}\quad \text{at}\quad z = 1 \tag{34}$$

As mentioned before, the set $\{f_i/1 \le i \le 10\}$ of simplifying coefficients used in Eqs. (28) - (31) are given by:

$$f_1 = \left(\frac{f_\mu}{f_\rho}\right)P_r\ ,\ f_2 = \left(\frac{f_{(\rho\beta)}}{f_\rho}\right)P_r\ ,\ f_3 = \left(\frac{1}{f_\rho}\right)R_NP_r\ ,$$
$$f_4 = \left(\frac{f_{\bar{\mu}}}{f_\rho}\right)\frac{P_r^2Q}{P_{rM}}\ ,\ f_5 = \frac{f_k}{f_{(\rho c)}}\ ,\ f_6 = \left(\frac{1}{f_{(\rho c)}}\right)N_b\ , \tag{35}$$
$$f_7 = \left(\frac{1}{f_{(\rho c)}}\right)N_t\ ,\ f_8 = \frac{1}{L_e}\ ,\ f_9 = \frac{N_t}{N_b\,L_e}\ ,f_{10} = \left(\frac{1}{f_{\bar{\mu}}\,f_\sigma}\right)\frac{P_r}{P_{rM}}\,.$$

Additionally, the relative thermophysical properties f_ρ , f_μ , $f_{\bar{\mu}}$, f_k, f_σ , $f_{(\rho\beta)}$ and $f_{(\rho c)}$ shown above are given by:

$$f_\rho = \frac{\rho_{nf}}{\rho_{bf}}\ ,\ f_\mu = \frac{\mu_{nf}}{\mu_{bf}}\ ,\ f_{\bar{\mu}} = \frac{\bar{\mu}_{nf}}{\bar{\mu}_{bf}}\ ,\ f_k = \frac{k_{nf}}{k_{bf}}\,,$$
$$f_\sigma = \frac{\sigma_{nf}}{\sigma_{bf}}\ ,\ f_{(\rho\beta)}\ = \frac{(\rho\beta)_{nf}}{(\rho\beta)_{bf}}\ ,\ f_{(\rho c)} = \frac{(\rho c)_{nf}}{(\rho c)_{bf}}\,. \tag{36}$$

The non-dimensional parameters R_a , R_N , Q , N_b , N_t , L_e , P_r and P_{rM} appeared in Eq. (35) represents the thermal Rayleigh number, the concentration Rayleigh number, the magnetic Chandrasekhar number, the Brownian motion parameter, the thermophoresis parameter, the Lewis number , the Prandtl number and the Magnetic Prandtl number, respectively. These non-dimensional physical quantities can be regarded as the pertinent parameters of the present stability problem , which are defined as follows:

$$R_a = \frac{(\rho\beta)_{bf}\,\Delta T g\,L^3}{\mu_{bf}\,\alpha_{bf}}\ ,\ R_N = \frac{\left(\rho_{np}-\rho_{bf}\right)gL^3\phi_0}{\mu_{bf}\,\alpha_{bf}}\,,$$
$$Q\ = \frac{\bar{\mu}_{bf}L^2H_0^2}{4\pi\eta_{bf}\,\mu_{bf}}\ ,\ N_b = \frac{D_B(\rho c)_{np}\phi_0}{\alpha_{bf}(\rho c)_{bf}}\ ,\ N_t = \frac{D_T(\rho c)_{np}\,\Delta T}{\alpha_{bf}(\rho c)_{bf}T_c}\,, \tag{37}$$
$$L_e = \frac{\alpha_{bf}}{D_B}\ ,\ P_r = \frac{\mu_{bf}}{\rho_{bf}\,\alpha_{bf}}\ ,\ P_{rM} = \frac{\mu_{bf}}{\rho_{bf}\,\eta_{bf}}\ .$$

Based on the aforementioned nanofluid models proposed for Al_2O_3-water nanofluids , the relative thermophysical properties f_ρ , f_μ , $f_{\bar{\mu}}$, f_k, f_σ , $f_{(\rho\beta)}$ and $f_{(\rho c)}$ in combination with the physical parameters R_N, L_e, N_b and N_t are accurately computed from Eqs. (36) and (37) and then summarized in Table 2 and Table 3, for varying values of d_{np} and ϕ_0. Here, these physical quantities are obtained by considering fixed values for the layer depth L , the reference temperature T_c and the temperature difference ΔT , where $0.01 \le \phi_0 \le 0.04$, $30\,nm \le d_{np} \le 45\,nm$, $L = 4.1\times10^{-5}m$, $T_c = 300K$ and $\Delta T = 1K$.

2.1 Basic Solutions

The thermo-magneto-hydrodynamic stability problem described by Eqs. (27) - (32) and the boundary conditions (33) and (34) has a steady state solution. In this particular state, the nanofluid is assumed to be at rest $\left(\text{i.e.},\mathbf{V_b} = (0,0,0)\right)$, in which the pressure P_b, the temperature T_b, the volumetric fraction of nanoparticles ϕ_b as well as the components $\left(H_{xb},H_{yb},H_{zb}\right)$ of the magnetic field $\mathbf{H_b}$ depend solely on z. Hence, under these restricted considerations, the basic state of the nanofluidic system is defined by:

$$\frac{dP_b}{dz}\ = f_2\,f_\rho R_aT_b - f_3f_\rho\,\phi_b - \frac{f_\rho\,P_r\,R_a}{\beta_{bf}\,\Delta T} \tag{38}$$

$$T_b = 1 - z \tag{39}$$

$$\phi_b = N_A\left(z - \frac{1}{2}\right) \tag{40}$$

$$\left(H_{xb},H_{yb},H_{zb}\right) = (0,0,1) \tag{41}$$

In addition to the above findings, it is important to mention here that the basic volumetric fraction ϕ_b of solid nanoparticles established in Eq. (40) is found analytically by taking into account the newest wakif's results (Wakif et al., 2016 , 2018a , 2018b , 2018c) concerning the revised nanofluid model, such that:

$$\bar{\phi}_b^* = \frac{1}{L}\int_0^L \phi_b^*dz^* = \phi_0 \tag{42}$$

$$\int_0^1 \phi_b dz = 0 \tag{43}$$

Global Digital Central
ISSN: 2151-8629

Here, $\bar{\phi}_b^*$ is the mean value of the dimensional volumetric fraction of nanoparticles ϕ_b^*.

2.2 Perturbation Equations

In order to examine the linear stability of the basic state defined previously by Eqs. (38) - (41) , it is more convenient to superimpose infinitesimal perturbations $\mathbf{V}'$, P' , T' , ϕ' and $\mathbf{H}'$ on the basic solutions $\mathbf{V_b}$, P_b , T_b , ϕ_b and $\mathbf{H_b}$, respectively , in such a way that:

$$\mathbf{V} = \mathbf{V}', P = P_b + P', T = T_b + T', \phi = \phi_b + \phi' , \mathbf{H} = \mathbf{e_z} + \mathbf{H}'. \quad (44)$$

Hence, after substituting the above expressions into Eqs. (27) - (32) and neglecting the nonlinear terms arising in the resulting differential system, we obtain the following linearized perturbation equations:

$$\nabla.\mathbf{V}' = 0 \quad (45)$$

$$\frac{\partial \mathbf{V}'}{\partial t} = -\frac{1}{f_\rho}\nabla P' + f_1 \nabla^2 \mathbf{V}' + \begin{bmatrix}(f_2 R_a T' - f_3 \phi')\mathbf{e_z} \\ +f_4(\nabla \times \mathbf{H}') \times \mathbf{e_z}\end{bmatrix} \quad (46)$$

$$\frac{\partial T'}{\partial t} - w' = f_5 \nabla^2 T' - \left(f_6 \frac{\partial \phi'}{\partial z} + f_7 \frac{\partial T'}{\partial z}\right) \quad (47)$$

$$\frac{\partial \phi'}{\partial t} + \frac{N_t}{N_b} w' = f_8 \nabla^2 \phi' + f_9 \nabla^2 T' \quad (48)$$

$$\frac{\partial \mathbf{H}'}{\partial t} = \frac{\partial \mathbf{V}'}{\partial z} + f_{10} \nabla^2 \mathbf{H}' \quad (49)$$

$$\nabla.\mathbf{H}' = 0 \quad (50)$$

For the resulting equations (45) - (50), the corresponding boundary conditions are stated as:

$$w' = \frac{\partial w'}{\partial z} = T' = \frac{\partial \phi'}{\partial z} + \frac{N_t}{N_b}\frac{\partial T'}{\partial z} = 0 \quad \text{at} \quad z = 0\,, 1 \quad (51)$$

By operating curl twice on Eq. (46), the pressure term P' can be assuredly removed from this equation. Hence, after some simplifications that take into account Eqs. (45) and (50), the z-components of Eqs. (46) and (49) can be formulated as follows:

$$\frac{\partial}{\partial t}(\nabla^2 w') = f_1 \nabla^4 w' + f_2 R_a \nabla_2^2 T' - f_3 \nabla_2^2 \phi' + f_4 \frac{\partial}{\partial z}(\nabla^2 H_z') \quad (52)$$

$$\frac{\partial H_z'}{\partial t} = \frac{\partial w'}{\partial z} + f_{10} \nabla^2 H_z' \quad (53)$$

Here, the operator ∇ represents the dimensionless gradient vector, whereas the dimensionless mathematical symbols ∇^2, ∇_2^2 and ∇^4 denote the usual Laplacian, horizontal Laplacian and bi-Laplacian operators, respectively, where $\nabla = (\partial/\partial x, \partial/\partial y, \partial/\partial z)$, $\nabla^2 = \nabla_2^2 + \partial^2/\partial z^2$, $\nabla_2^2 = \partial^2/\partial x^2 + \partial^2/\partial y^2$ and $\nabla^4 = \nabla^2(\nabla^2)$.

2.3 Normal Mode Analysis

Due to the existence of periodic solutions, the normal mode analysis is adopted as a useful means to study the linear stability of the present nanofluidic system. Accordingly, the small quantities w' ,T', ϕ' and H_z' can then be analyzed into two-dimensional waves by considering time-dependent periodic disturbances , which are characterized by particular wave numbers a_x and a_y .Therefore, the disturbances w' ,T', ϕ' and H_z' can be written in the following form:

$$\begin{bmatrix} w' \\ T' \\ \phi' \\ H_z' \end{bmatrix} = \begin{bmatrix} \mathcal{w}(z) \\ \theta(z) \\ \Phi(z) \\ \mathcal{H}(z) \end{bmatrix} exp\left[i\left(a_x x + a_y y\right) + \lambda t\right] \quad (54)$$

Consequently, after substituting Eq. (54) into Eqs. (47), (48), (52) and (53), we get the following stability equations:

$$\begin{bmatrix} f_1(D^4 - 2a^2D^2 + a^4)\mathcal{w} \\ -f_2 R_a a^2 \theta + f_3 a^2 \Phi \end{bmatrix} + f_4(D^3 - a^2 D)\mathcal{H} = \lambda\,(D^2 - a^2)\mathcal{w} \quad (55)$$

$$\mathcal{w} + (f_5 D^2 - f_7 D - f_5 a^2)\theta - f_6\, D\Phi = \lambda\theta \quad (56)$$

$$-\frac{N_t}{N_b}\mathcal{w} + f_9\,(D^2 - a^2)\theta + f_8(D^2 - a^2)\Phi = \lambda\Phi \quad (57)$$

$$D\mathcal{w} + f_{10}(D^2 - a^2)\mathcal{H} = \lambda\mathcal{H} \quad (58)$$

Here, a shows the dimensionless wave number in the x-y plane and D^n represents the n^{th}- order derivative with respect to the variable z, where $a = \left(a_x^2 + a_y^2\right)^{0.5}$ and $D^n = d^n/dz^n$.

By assuming that the principle of exchange of stabilities is valid for the present thermo-magneto-hydrodynamic stability problem and the stationary convection (i.e., $\lambda = 0$) is the solely considered mode, the system of Eqs. (55) - (58) can be reduce to the following eigenvalue problem:

$$\begin{pmatrix} A_{\mathcal{w}} & 0 & f_3\, a^2 \\ 1 & B_\theta & B_\Phi \\ -N_t/N_b & C_\theta & C_\Phi \end{pmatrix}\begin{pmatrix}\mathcal{w} \\ \theta \\ \Phi\end{pmatrix} = R_a \begin{pmatrix} 0 & f_2\, a^2 & 0 \\ 0 & 0 & 0 \\ 0 & 0 & 0 \end{pmatrix}\begin{pmatrix}\mathcal{w} \\ \theta \\ \Phi\end{pmatrix} \quad (59)$$

Additionally, the differential operators $A_{\mathcal{w}}$, B_θ , B_Φ , C_θ and C_Φ shown above are expressed as follows:

$$A_{\mathcal{w}} = f_1 D^4 - \left(2f_1 a^2 + \frac{f_4}{f_{10}}\right)D^2 + f_1 a^4 \quad (60)$$

$$B_\theta = f_5 D^2 - f_7 D - f_5\, a^2 \quad (61)$$

$$B_\Phi = -f_6\, D \quad (62)$$

$$C_\theta = f_9\,(D^2 - a^2) \quad (63)$$

$$C_\Phi = f_8(D^2 - a^2) \quad (64)$$

In view of the linear stability theory and normal mode analysis, the boundary conditions (51) become:

$$\mathcal{w} = D\mathcal{w} = \theta = D\Phi + \frac{N_t}{N_b} D\theta = 0 \quad \text{at} \quad z = 0\,, 1 \quad (65)$$

From the computational point of view, the criterion for the onset magneto-convection in Al_2O_3 - water nanofluids can be examined efficiently after converting the Neumann boundary condition for the nanoparticles $D\Phi + (N_t/N_b)D\theta = 0$ into a Dirichlet type boundary condition. For this purpose, it is more useful to apply a suitable change in the mathematical formulation of the problem by considering a new variable Γ instead of Φ . Based on the latest work of Wakif et al. (2018b), this modification can be easily made by setting the imposed change of variable $\Gamma = -D\Phi - (N_t/N_b)D\theta$. In view of this consideration, the eigenvalue problem described by Eq. (59) becomes:

$$\begin{pmatrix} \bar{A}_{\mathcal{w}} & -R_N N_t\, a^2/N_b & \bar{A}_\Gamma \\ f_{(\rho c)} & \bar{B}_\theta & N_b \\ \bar{C}_w & 0 & \bar{C}_\Gamma \end{pmatrix}\begin{pmatrix}\mathcal{w} \\ \theta \\ \Gamma\end{pmatrix} = R_a \begin{pmatrix} 0 & f_{(\rho\beta)}\, a^2 & 0 \\ 0 & 0 & 0 \\ 0 & 0 & 0 \end{pmatrix}\begin{pmatrix}\mathcal{w} \\ \theta \\ \Gamma\end{pmatrix} \quad (66)$$

Here, the modified differential operators $\bar{A}_{\mathcal{w}}$, $\bar{A}_\Gamma$, $\bar{B}_\theta$, $\bar{C}_w$ and $\bar{C}_\Gamma$ are given explicitly by :

$$\bar{A}_{\mathcal{w}} = f_\mu D^4 - \left(2\, f_\mu a^2 + Q\, f_\sigma f_{\bar{\mu}}^2\right)D^2 + \left(f_\mu a^4 - \frac{R_N N_t L_e}{N_b}\right) \quad (67)$$

$$\bar{A}_\Gamma = -R_N D \quad (68)$$

$$\bar{B}_\theta = f_k(D^2 - a^2) \quad (69)$$

Global Digital Central
ISSN: 2151-8629

$$\bar{C}_w = \frac{L_e N_t}{N_b} D \tag{70}$$

$$\bar{C}_\Gamma = D^2 - a^2 \tag{71}$$

For the resulting eigenvalue problem (66), the associated boundary conditions are written as follows:

$$w = Dw = \theta = \Gamma = 0 \quad \text{at} \quad z = 0\,, 1 \tag{72}$$

Table 2 Computed values of f_ρ , f_μ , $f_{\bar{\mu}}$, f_k , f_σ , $f_{(\rho\beta)}$ and $f_{(\rho c)}$, for different values of d_{np} and ϕ_0 .

d_{np}	ϕ_0	f_ρ	f_μ	$f_{\bar{\mu}}$	f_k	f_σ	$f_{(\rho\beta)}$	$f_{(\rho c)}$
30 nm	0.01	1.02981	1.08960	0.99999	1.04922	0.98507	0.99161	0.99728
	0.02	1.05963	1.20181	0.99999	1.08255	0.97029	0.98322	0.99457
	0.03	1.08944	1.34222	0.99999	1.11171	0.95566	0.97483	0.99186
	0.04	1.11926	1.52185	0.99999	1.13845	0.94117	0.96644	0.98915
35 nm	0.01	1.02981	1.08520	0.99999	1.04650	0.98507	0.99161	0.99728
	0.02	1.05963	1.19095	0.99999	1.07798	0.97029	0.98322	0.99457
	0.03	1.08944	1.32178	0.99999	1.10553	0.95566	0.97483	0.99186
	0.04	1.11926	1.48679	0.99999	1.13079	0.94117	0.96644	0.98915
40 nm	0.01	1.02981	1.08158	0.99999	1.04426	0.98507	0.99161	0.99728
	0.02	1.05963	1.18208	0.99999	1.07423	0.97029	0.98322	0.99457
	0.03	1.08944	1.30529	0.99999	1.10046	0.95566	0.97483	0.99186
	0.04	1.11926	1.45890	0.99999	1.12450	0.94117	0.96644	0.98915
45 nm	0.01	1.02981	1.07853	0.99999	1.04238	0.98507	0.99161	0.99728
	0.02	1.05963	1.17466	0.99999	1.07108	0.97029	0.98322	0.99457
	0.03	1.08944	1.29160	0.99999	1.09618	0.95566	0.97483	0.99186
	0.04	1.11926	1.43602	0.99999	1.11921	0.94117	0.96644	0.98915

Table 3 Effective values of the parameters R_N , L_e , N_b and N_t , for different values of d_{np} and ϕ_0 .

d_{np}	ϕ_0	R_N	$L_e(\times 10^4)$	$N_b(\times 10^{-6})$	$N_t(\times 10^{-6})$
30 nm	0.01	0.15336	0.89376	0.81548	0.56988
	0.02	0.30672	0.89376	1.63097	1.13976
	0.03	0.46008	0.89376	2.44646	1.70964
	0.04	0.61344	0.89376	3.26194	2.27952
35 nm	0.01	0.15336	1.04272	0.69898	0.56988
	0.02	0.30672	1.04272	1.39797	1.13976
	0.03	0.46008	1.04272	2.09696	1.70964
	0.04	0.61344	1.04272	2.79595	2.27952
40 nm	0.01	0.15336	1.19168	0.61161	0.56988
	0.02	0.30672	1.19168	1.22323	1.13976
	0.03	0.46008	1.19168	1.83484	1.70964
	0.04	0.61344	1.19168	2.44646	2.27952
45 nm	0.01	0.15336	1.34064	0.54365	0.56988
	0.02	0.30672	1.34064	1.08731	1.13976
	0.03	0.46008	1.34064	1.63097	1.70964
	0.04	0.61344	1.34064	2.17463	2.27952

Global Digital Central
ISSN: 2151-8629

3. NUMERICAL SOLUTION

3.1 Solution Methodology

As already mentioned , the obtained linear eigenvalue problem (66) in association with the reduced boundary conditions (72) can be handled numerically by discretizing their ordinary differential equations along the z-direction. Consequently, after choosing an appropriate discretization scheme, the continuous stationary differential equations arising from the present stability problem are treated mathematically with their associated boundary conditions (72) as a generalized algebraic eigenvalue problem, whose eigenvalues constitute a discrete set of all possible values of the control parameter R_a. In this regards, it bears mentioning here that the thermal Rayleigh number R_a corresponding to a fixed wave number a is selected in such a way to be the smallest value among all positive real eigenvalues. Moreover, this possible value depends greatly on the values of the control parameters ϕ_0 , d_{np} and Q characterizing the nanofluidic system.

Accordingly, in order to find the underlying relationship between the thermal Rayleigh number R_a and the wave number a corresponding to the stationary mode of convection, we adopt an efficient tool that can yield more accurate results. In view of this, the physical domain is converted from $[0\ 1]$ to the space interval $[-1\ 1]$ by replacing the space variable z with another variable ξ, where $\xi = 2z - 1$. At this stage, the main unknowns w, θ and Γ are transformed to $\bar{w}$, $\bar{\theta}$ and $\bar{\Gamma}$, respectively, such that $\bar{w} = w\left(z(\xi)\right)$, $\bar{\theta} = \theta\left(z(\xi)\right)$, $\bar{\Gamma} = \Gamma\left(z(\xi)\right)$ and $D^n X = 2^n \bar{D}^n \bar{X}$, where n is an integer derivative order and X is an unknown of the problem (i.e., w, θ or Γ) with $\bar{D}^n = d^n/d\xi^n$. Keeping in mind this mathematical considerations, the computational domain $[-1\ 1]$ is discretized non-uniformly into a set of $(N-1)$ successive sub-domains $[\xi_{i+1}\ \xi_i]$ by utilizing the Gauss-Lobatto grid collocation points, in such a way that $\xi_i = cos[\pi(i-1)/(N-1)]$ and $\xi_N \le \xi_i \le \xi_1$, where i is an integer index varying decreasingly from $(N-1)$ to 1 and N is the total number of collocation points chosen in the numerical implementation.

Hence, based on the Gauss-Lobatto grid collocation points and the Chebyshev polynomial interpolation, the derivatives of the function $\bar{X}(\xi)$ with respect to the variable ξ at a collocation point ξ_i are expressed by:

$$\bar{D}^n \bar{X}(\xi_i) = \sum_{j=1}^{N} \tilde{d}_{ij}^{(n)}\, \bar{X}(\xi_j) = \sum_{j=1}^{N} \tilde{d}_{ij}^{(n)}\, \bar{X}_j \tag{73}$$

In addition, the discrete solutions $\{(\bar{w}_i, \bar{\theta}_i, \bar{\Gamma}_i)/2 \le i \le N-1\}$ at each collocation point ξ_i can be found through the following resulting algebraic eigenvalue problem:

$$\begin{pmatrix} \bar{A}_{ij}^{\bar{w}} & -R_N N_t\, a^2 \delta_{ij}/N_b & \bar{A}_{ij}^{\bar{\Gamma}} \\ f_{(\rho c)}\delta_{ij} & \bar{B}_{ij}^{\bar{\theta}} & N_b \delta_{ij} \\ \bar{C}_{ij}^{\bar{w}} & Z_{ij} & \bar{C}_{ij}^{\bar{\Gamma}} \end{pmatrix} \begin{pmatrix} \bar{w}_j \\ \bar{\theta}_j \\ \bar{\Gamma}_j \end{pmatrix} = R_a \begin{pmatrix} Z_{ij} & f_{(\rho\beta)}\, a^2 \delta_{ij} & Z_{ij} \\ Z_{ij} & Z_{ij} & Z_{ij} \\ Z_{ij} & Z_{ij} & Z_{ij} \end{pmatrix} \begin{pmatrix} \bar{w}_j \\ \bar{\theta}_j \\ \bar{\Gamma}_j \end{pmatrix} \tag{74}$$

Here, δ_{ij} represents the Kronecker symbol, where $2 \le i, j \le N-1$. Furthermore, the elements $\bar{A}_{ij}^{\bar{w}}$, $\bar{A}_{ij}^{\bar{\Gamma}}$, $\bar{B}_{ij}^{\bar{\theta}}$, $\bar{C}_{ij}^{\bar{w}}$, $\bar{C}_{ij}^{\bar{\Gamma}}$, Z_{ij} shown above are expressed formally by:

$$\bar{A}_{ij}^{\bar{w}} = 16\, f_\mu \tilde{D}_{ij}^{(4)} + \begin{bmatrix} -4\left(2 f_\mu a^2 + Q\, f_\sigma f_{\bar{\mu}}^2\right)\tilde{D}_{ij}^{(2)} \\ +\left(f_\mu a^4 - \dfrac{R_N N_t L_e}{N_b}\right)\delta_{ij} \end{bmatrix} \tag{75}$$

$$\bar{A}_{ij}^{\bar{\Gamma}} = -2R_N\, \tilde{d}_{ij}^{(1)} \tag{76}$$

$$\bar{B}_{ij}^{\bar{\theta}} = f_\kappa\left(4\, \tilde{d}_{ij}^{(2)} - a^2 \delta_{ij}\right) \tag{77}$$

$$\bar{C}_{ij}^{\bar{w}} = \frac{2\, L_e N_t}{N_b}\, \tilde{D}_{ij}^{(1)} \tag{78}$$

$$\bar{C}_{ij}^{\bar{\Gamma}} = 4\, \tilde{d}_{ij}^{(2)} - a^2 \delta_{ij} \tag{79}$$

$$Z_{ij} = 0 \tag{80}$$

According to Canuto et al. (2012) , the elements $\tilde{d}_{ij}^{(1)}$ of the first-order Chebyshev differentiation matrix $\tilde{\mathbf{D}}^{(1)}$ are given by:

$$\tilde{d}_{ij}^{(1)} = \begin{cases} (2N^2 - 4N + 3)/6 & \text{for} \quad i = j = 1 \\ \xi_i / \left(2\xi_i^2 - 2\right) & \text{for} \quad i = j \neq 1, N \\ (-1)^{i+j} c_i / \left(c_j \xi_i - c_j\, \xi_j\right) & \text{for} \quad i \neq j \\ (-2N^2 + 4N - 3)/6 & \text{for} \quad i = j = N \end{cases} \tag{81}$$

Here, the coefficients c_i are defined as follows:

$$c_i = \begin{cases} 2 & \text{for} \quad i = 1, N \\ 1 & \text{for} \quad i \neq 1, N \end{cases} \tag{82}$$

In view of the Chebyshev-Gauss-Lobatto Spectral Method, the other elements $\tilde{d}_{ij}^{(n)}$ corresponding to the n^{th}- order Chebyshev differentiation matrix $\tilde{\mathbf{D}}^{(n)}$ can be computed recurrently as follows:

$$\tilde{d}_{ij}^{(n)} = \sum_{k=1}^{N} \tilde{d}_{ik}^{(n-1)}\, \tilde{d}_{kj}^{(1)} \tag{83}$$

Based on the mathematical techniques reported by Trefethen (2000) and the boundary conditions $w = 0$ and $Dw = 0$, the other elements $\tilde{D}_{ij}^{(1)}$, $\tilde{D}_{ij}^{(2)}$ and $\tilde{D}_{ij}^{(4)}$ used above are computed analytically from the basic elements $\tilde{d}_{ij}^{(1)}$,$\tilde{d}_{ij}^{(2)}$, $\tilde{d}_{ij}^{(3)}$and $\tilde{d}_{ij}^{(4)}$ as follows :

$$\tilde{D}_{ij}^{(1)} = \frac{1}{\left(1 - \xi_i^2\right)}\left[\left(1 - \xi_i^2\right)\tilde{d}_{ij}^{(1)} - 2\xi_i \delta_{ij}\right] \tag{84}$$

$$\tilde{D}_{ij}^{(2)} = \frac{1}{\left(1 - \xi_i^2\right)}\left[\left(1 - \xi_i^2\right)\tilde{d}_{ij}^{(2)} - 4\xi_i \tilde{d}_{ij}^{(1)} - 2\delta_{ij}\right] \tag{85}$$

$$\tilde{D}_{ij}^{(4)} = \frac{1}{\left(1 - \xi_i^2\right)}\left[\left(1 - \xi_i^2\right)\tilde{d}_{ij}^{(4)} - 8\xi_i \tilde{d}_{ij}^{(3)} - 12\tilde{d}_{ij}^{(2)}\right] \tag{86}$$

As proved above, the generalized algebraic eigenvalue problem described by Eq. (74) has $(3N-6)$ eigenvalues γ_i . These characteristic values depend implicitly upon several parameters, including the wave number a , the volumetric fraction of nanoparticles ϕ_0 , the diameter of nanoparticles d_{np} as well as the magnetic Chandrasekhar number Q . Hence, for specified values of these physical parameters , the possible eigenvalues γ_i can be found numerically for each fixed wave number a , in such a way that the sought thermal Rayleigh number R_a must be the smallest eigenvalue among the whole set of positive real eigenvalues (i.e., $R_a = min\{\gamma_i/\gamma_i > 0\}$) . After employing the Golden Section Search Method (GSSM), we can find the critical stability parameters R_{ac} and a_c by minimizing numerically R_a with respect to a in a wide interval $[a_i\ a_f]$ (e.g., $a \in [0\ \ 10]$).

3.2 Numerical, Analytical and Semi-Analytical Validations

As discussed above, for analyzing the thermo-magneto-hydrodynamic instability occurred in a thin horizontal layer of a nanofluid, several numerical implementations have been performed for of Al_2O_3- water nanofluids using Chebyshev-Gauss-Lobatto Spectral Method (CGLSM). Recently, this method attracts extensive attention from researchers due to its importance in a wide range of applications as a fast, flexible and accurate numerical procedure to solve the linear and nonlinear problems

in fluid mechanics and other related areas. Hence, in order to verify the correctness and reliability of our present numerical findings in terms of the critical stability parameters R_{ac} and a_c , a detailed side-by-side comparison has been carried out using Chebyshev-Gauss-Lobatto Spectral Method (CGLSM) and Generalized Differential Quadrature Method (GDQM). Moreover, it is worth mentioning here that GDQM is exceptionally used in this investigation as a comparative numerical method to validate our results. To the best of our knowledge, no previous studies have systematically examined by means of GDQM to solve similar stability problems. Hence, in order to provide extensive details about this numerical method, the readers can refer to the book of Shu (2012). Also, the interested researchers can see the innovative works of Fidanoglu et al. (2014) , Qasim et al. (2018) and the references therein, in which GDQM is explained more fully through two different practical situations. Based on our CGLSM and GDQM codes, the results are presented in tabular and graphical forms to discuss the significant effects of the emerging parameters Q , ϕ_0 and d_{np} on the thermo-magneto-hydrodynamic stability of Al_2O_3- water nanofluids as well as to quantify the agreement between the results of these numerical methods. As shown in Fig. 2 , Fig. 3 , Fig. 4 , Fig. 5 , Fig. 6 and Table 4, it is found that the graphical and tabular results given by CGLSM are very close to those of GDQM, which lends further credibility to our final outcomes and also emphasizes the robustness and validity of the CGLSM code.

In the aim to authenticate the accuracy of our numerical results generated by the aforementioned collocation numerical methods and verify the efficiency of the computational codes used in this investigation towards some limiting cases for computing the critical values of the parameters R_a and a , we first compare the results of our CGLSM and GDQM codes with those obtained analytically by Chandrasekhar (1961) and numerically by Wakif et al. (2018b) using Variational Method (VM) and Runge-Kutta-Fehlberg Method (RKFM), respectively, for the case of electrically conducting fluids (i. e. , $\phi_0 = 0$) as shown in Table 5.

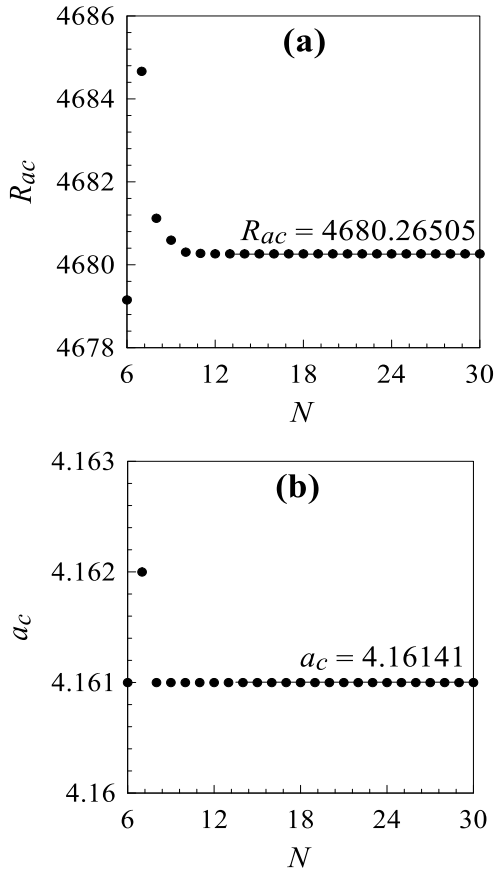

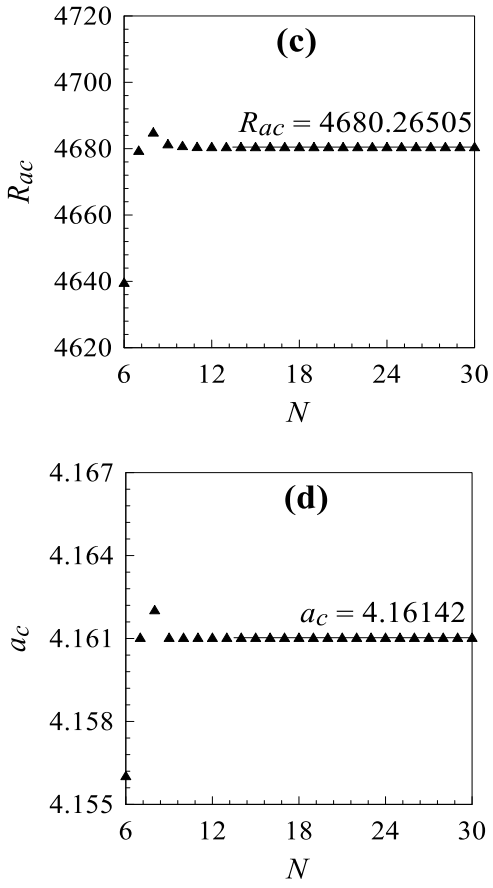

Fig. 2 Convergence test for R_{ac} and a_c using **(a,b)** CGLSM and **(c,d)** GDQM, when $Q = 200$, $\phi_0 = 0.01$ and $d_{np} = 30nm$.

In the second set of examination tests, we compare in Table 6 our numerical results given by CGLSM and GDQM with those obtained semi-analytically with the help of Wakif-Galerkin Weighted Residuals Technique (WGWRT) based on the revised Buongiorno's two-phase classical model, in the case of electrically conducting nanofluids, where $f_\rho = f_\mu = f_{\bar{\mu}} = f_k = f_\sigma = f_{(\rho\beta)} = f_{(\rho c)} = 1$.

For a more explanation and detailed description of WGWRT , the interested reader is strongly encouraged to refer to the pioneering work of Wakif et al. (2018c), in which WGWRT is used as a semi-analytical method for analyzing the onset of electro-convection in dielectric nanofluids.

As expected, it is clearly seen from Table 5 and Table 6 that the numerical results of CGLSM and GDQM have an excellent degree of agreement with those of VM, RKFM and WGWRT. Consequently, the validation of our results is confirmed numerically, analytically and semi-analytically with a very high degree of precision.

Moreover, Fig. 2 is plotted for Al_2O_3- water nanofluids to control the convergence efficiency of CGLSM and GDQM in terms of the critical stability parameters R_{ac} and a_c. From this graphical representation, it is clearly observed that the convergence curves obtained by CGLSM and GDQM can be stabilized when the number of collocation points N exceeds a certain value N_0. As a result, it is noticed graphically from Fig. 2 that $N_0 = 10$, in the case where $Q = 200$, $\phi_0 = 0.01$ and $d_{np} = 30\ nm$.

In order to achieve an absolute accuracy of the order of 10^{-6}, it is more recommended to take $N = 28$ for the number of collocation points during all subsequent analyses by CGLSM and GDQM. Furthermore, it

Global Digital Central
ISSN: 2151-8629

is found that the average CPU time taken for computing the accurate critical stability parameters R_{ac} and a_c by CGLSM or GDQM is no more than 40 s.

4. ANALYSIS OF RESULTS

In the present numerical investigation, the onset of thermo-magneto-hydrodynamic instability in Al_2O_3- water nanofluids is analyzed more realistically for non-slip , zero nanoparticles mass flux and isothermal boundary conditions, in such a way that the effects of Brownian motion and thermophoresis of nanoparticles are taken into account by using Buongiorno's two-phase nanofluid model with variable thermophysical properties.

Based on the linear stability analysis and the normal mode method, the set of the governing partial differential equations along with their corresponding boundary conditions are carefully transformed into a generalized algebraic eigenvalue problem with the help of Chebyshev-Gauss-Lobatto Spectral Method (CGLSM), in order to solve this problem numerically by means of the Golden Section Search Method (GSSM). Additionally, all the results given by our CGLSM algorithm are validated numerically against those obtained using Generalized Differential Quadrature Method (GDQM).

The generated CGLSM and GDQM codes used in this investigation are further tested and multiply validated (i.e., numerically, analytically and semi-analytically) for some limiting cases using other powerful existing methods, such as Variational Method (VM), Runge-Kutta-Fehlberg Method (RKFM) and Wakif-Galerkin Weighted Residuals Technique (WGWRT).

Moreover, the effects of some parameters including the magnetic Chandrasekhar number Q , the volumetric fraction ϕ_0 and the diameter d_{np} of alumina nanoparticles on the onset of magneto-convection in a thin horizontal layer filled with alumina - water nanofluid are examined numerically by CGLSM and GDQM via various graphical illustrations as highlighted in Fig. 3 and Fig. 4. In these figures, the variations of the critical stability parameters R_{ac} and a_c as a function of the magnetic Chandrasekhar number Q are plotted and discussed for multiple values of the pertinent parameters ϕ_0 and d_{np} , where $200 \leq Q \leq 1000$, $0.01 \leq \phi_0 \leq 0.04$ and $30nm \leq d_{np} \leq 45nm$.

Furthermore, it is worth mentioning here that the graphical curves and tabular results highlighted in Fig. 3 , Fig. 4 and Table 4 are re-illustrated in another way in Fig. 5 and Fig. 6, in order to facilitate the stability analysis of Al_2O_3- water nanofluids.

Additionally, the rates of increase or decrease for the tabulated functions $R_{ac} = g_1(Q)$, $a_c = h_1(Q)$, $R_{ac} = g_2(\phi_0)$, $a_c = h_2(\phi_0)$, $R_{ac} = g_3(d_{np})$, $a_c = h_3(d_{np})$ and $R_{ac} = f(a_c)$ are estimated numerically by computing the slopes of their corresponding data, respectively, using the linear regression model (Makinde et al., 2018 ; Animasaun and Pop , 2017; Shah et al., 2018) as shown in Table 4.

The effect of the presence of an externally applied magnetic field on the critical stability parameters R_{ac} and a_c characterizing the onset of magneto-convection in Al_2O_3- water nanofluids is exhibited clearly in Fig. 3 and Fig. 4 by varying the magnetic Chandrasekhar number Q . In these graphical illustrations, the variations of R_{ac} and a_c are depicted as a function of the magnetic Chandrasekhar number Q , for different values of the parameters ϕ_0 and d_{np}.

As seen in Fig. 3 and Fig. 4, it is obviously observed that the critical thermal Rayleigh number R_{ac} increases with the simultaneous elevation of the magnetic Chandrasekhar number Q. Physically, this fact is mainly happened due to the Lorentzian magnetic drag force generated by the magnetic field in the electrically conducting medium. Likewise, this magnetic force has a resistive behavior, which acts to oppose and slow down the nanofluid flow caused by the imposed heating gradient $\Delta T/L$. In view of this, it is concluded that the thermo-magneto-hydrodynamic stability of Al_2O_3-water nanofluid can be affected by applying a uniform transverse magnetic field to a horizontal thin layer of this electrically conducting nanofluid. Hence, the onset of magneto-convection in the medium can be delayed under the influence of the magnetic field strength H_0, in such a way that the nanofluidic system becomes more stable with increasing the magnetic Chandrasekhar number Q. Similarly, it is noticed from the same figures that the critical wave number a_c can be increased by intensifying the magnetic field strength H_0, indicating that the thermo-magneto-hydrodynamic stability of Al_2O_3- water nanofluids caused by the increase in the magnetic Chandrasekhar number Q is accompanied by a significant reduction in the critical size of convection cells L_c $(i.e., L_c = 2\pi/a_c)$.

As shown in Table 2 and Table 3, the effect of adding alumina nanoparticles Al_2O_3 into a pure water H_2O has a major influence on the thermophysical properties of the resulting nanofluid. This subsequently affects the physical control parameters R_N , N_b and N_t characterizing respectively the significant impact of nanoparticles volume fraction, Brownian motion and thermophoresis of alumina nanoparticles on the thermo-magneto-hydrodynamic stability of Al_2O_3 - water nanofluids.

From Table 2, it can be concluded that the increasing amount of alumina nanoparticles Al_2O_3 inserted into the pure water is the most important factor responsible for significant enhancement in the heat transfer rate efficiency of Al_2O_3- water nanofluid, due to the fact that the thermal conductivity of this nanofluid is an increasing function of the volumetric fraction ϕ_0. In view of this fact, it can be concluded from Table 3 that raising the volumetric fraction ϕ_0 of alumina nanoparticles Al_2O_3 brings about a noteworthy boost in the Brownian motion and thermophoresis effects, which yields significant random movement of alumina nanoparticles Al_2O_3 throughout the whole medium. Therefore, keeping that in mind, the nanofluidic system becomes more unstable due to the intensive disturbances exerted by the nanoparticles flow in the nanofluid layer. Hence, the volumetric fraction of nanoparticles ϕ_0 has a destabilizing effect on the nanofluidic system. This physical analysis is consistent with the graphical results depicted in Fig. 3, in which the onset of magneto-convection in alumina-water nanofluids can be hasten by adding alumina nanoparticles Al_2O_3 in the nanofluidic medium in very small amounts. Also, it is revealed from this graphical content that there is a marked enhancement in the critical size of convection cells L_c . These results are happened due to the significant decrease in the critical stability parameters R_{ac} and a_c during the concentration increase.

Fig. 4 is plotted to explore the influence of alumina nanoparticles dimension d_{np} on the critical values R_{ac} and a_c characterizing the onset of thermo-magneto-hydrodynamic instability and the critical size of convection cells, respectively. As for the previous graphical illustrations, it is observed similar behaviors in Fig. 4 for the diameter d_{np} of alumina nanoparticles Al_2O_3 on the critical stability parameters R_{ac} and a_c . Consequently, the rise in the diameter d_{np} has a destabilizing effect on the nanofluidic system. Besides this, the onset of the magneto-convection in alumina - water nanofluids is accelerated and the critical size of convection cells L_c is increased due to the increase in the diameter d_{np}. Additionally, it can be noticed from the expressions of Lewis number L_e and Table 3 that there is a direct proportionality between L_e and d_{np}. Therefore, these parameters have the same influence on the thermo-magneto-hydrodynamic stability of Al_2O_3- water nanofluids.

As a remark, it is worth mentioning here that the limiting case of electrically conducting fluids is highlighted graphically by $\phi_0 = 0$ and $d_{np} = 0$ as shown in Fig. 3 and Fig. 4, respectively. Based on these graphical presentations, it can be noted that the electrically conducting fluids are more stable than the electrically conducting nanofluids. Also, the key results arising from the present numerical investigation are summarized graphically as shown in Fig. 5 and Fig. 6.

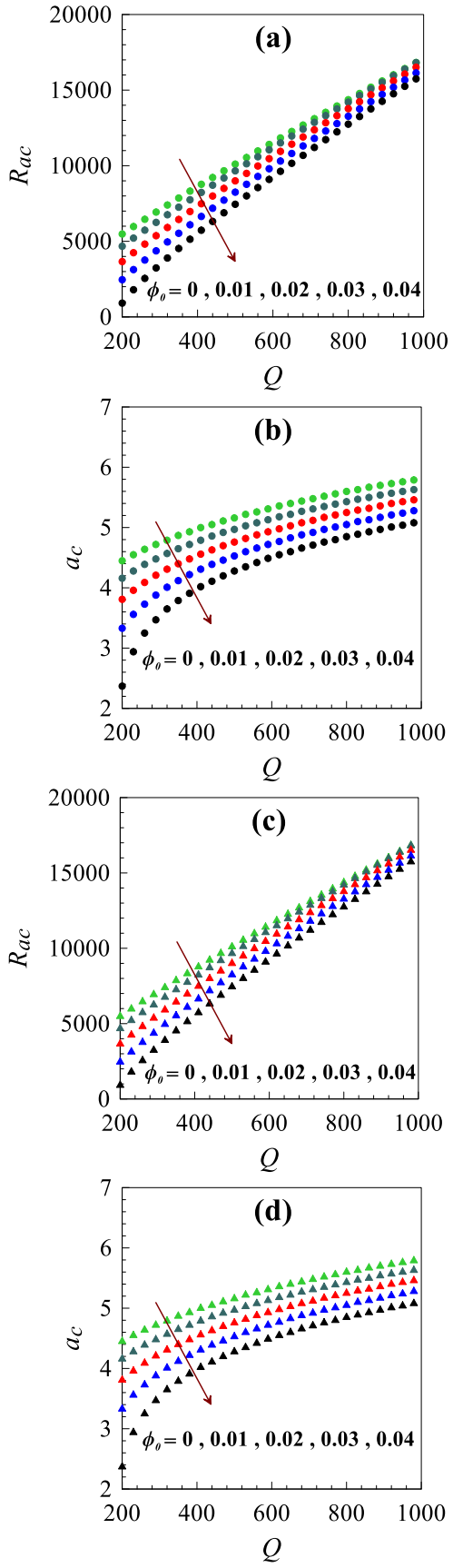

Fig. 3 Examination of the influence of Q and ϕ_0 on R_{ac} and a_c by means of (**a,b)** CGLSM and **(c,d)** GDQM, when $d_{np} = 30nm$.

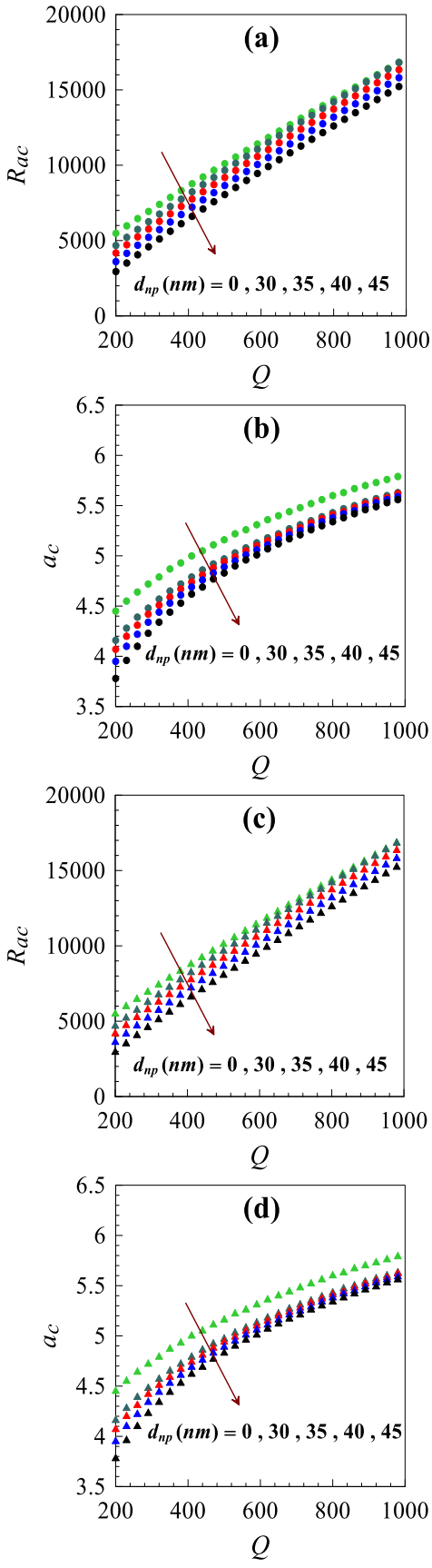

Fig. 4 Examination of the influence of Q and d_{np} on R_{ac} and a_c by means of (**a,b)** CGLSM and **(c,d)** GDQM, when $\phi_0 = 0.01$.

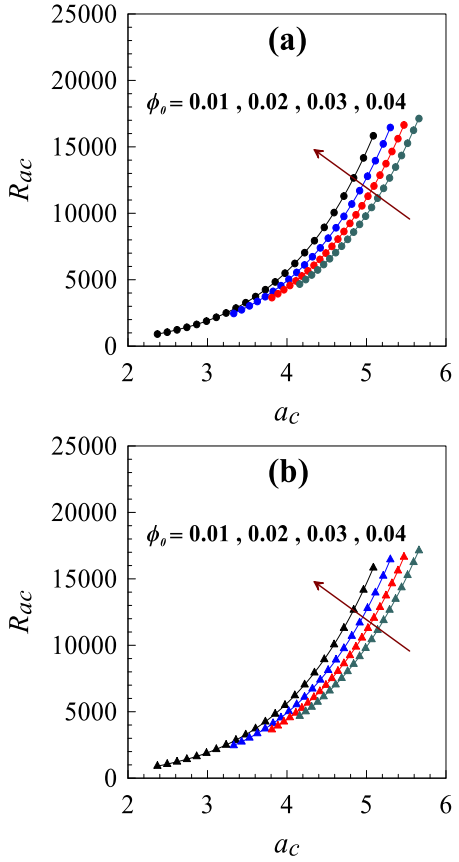

Fig. 5 Numerical determination of the variation of R_{ac} with respect to a_c, for increasing values of Q $(200 \leq Q \leq 1000)$ and various values of ϕ_0 using **(a)** CGLSM and **(b)** GDQM, when $d_{np} = 30nm$.

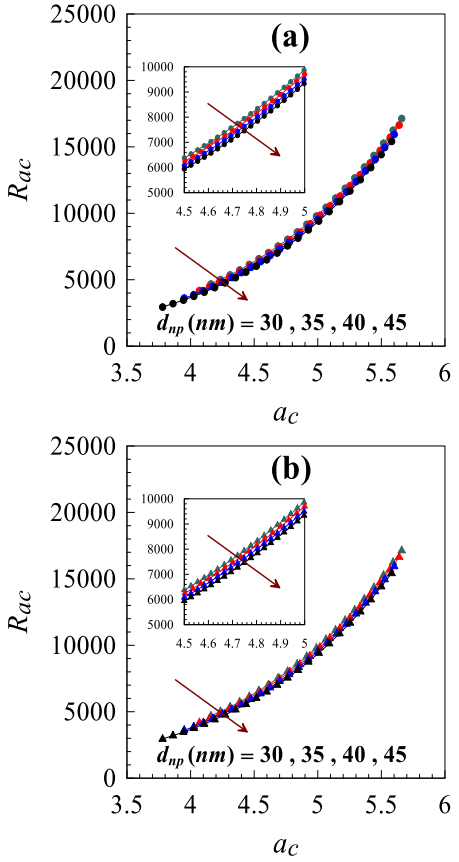

Fig. 6 Numerical determination of the variation of R_{ac} with respect to a_c, for increasing values of Q $(200 \leq Q \leq 1000)$ and various values of d_{np} using **(a)** CGLSM and **(b)** GDQM, when $\phi_0 = 0.01$.

Table 4 Numerical estimation of R_{ac} and a_c with the help of CGLSM and GDQM, for various values of Q, ϕ_0 and d_{np}.

Q	ϕ_0	$d_{np}(nm)$	Present Numerical Results			
			CGLSM		GDQM	
			R_{ac}	a_c	R_{ac}	a_c
200	0.01	30	4680.26505	4.16141	4680.26505	4.16142
500			9665.04216	4.97386	9665.04216	4.97383
700			12720.09144	5.29646	12720.09144	5.29649
1000			17107.11916	5.65539	17107.11916	5.65540
Slope1 for $R_{ac} = g_1(Q)$ and $a_c = h_1(Q)$			**15,51837**	**0,00185**	**15,51837**	**0,00185**
Slope2 for $R_{ac} = f(a_c)$			**8071,95022**		**8071,92481**	
500	**0.01**	35	9190.50576	4.93653	9190.50576	4.93652
	0.02		8004.13357	4.67673	8004.13357	4.67673
	0.03		6663.78341	4.37595	6663.78341	4.37598
	0.04		5175.71261	4.01388	5175.71262	4.01386
Slope1 for $R_{ac} = g_2(\phi_0)$ and $a_c = h_2(\phi_0)$			**-133847,29610**	**-30,68730**	**-133847,29580**	**-30,68730**
Slope2 for $R_{ac} = f(a_c)$			**4353,65216**		**4353,63155**	
700	0.02	**30**	12220.32039	5.10955	12220.32039	5.10950
		35	11231.94926	5.05038	11231.94926	5.05039
		40	10120.77628	4.97275	10120.77628	4.97275
		45	8877.84191	4.87224	8877.84191	4.87221
Slope1 for $R_{ac} = g_3(d_{np})$ and $a_c = h_3(d_{np})$			**-222,77216**	**-0,01579**	**-222,77216**	**-0,01579**
Slope2 for $R_{ac} = f(a_c)$			**13999,50057**		**13999,73352**	

Table 5 Comparison of our numerical results with the Chandrasekhar's and Wakif's results, in the case of electrically conducting fluids (i. e., $\phi_0 = 0$).

Q	Existing Literature Results				Present Numerical Results			
	VM (Chandrasekhar, 1961)		RKFM (Wakif et al., 2018b)		CGLSM (N = 15)		GDQM (N = 15)	
	R_{ac}	a_c	R_{ac}	a_c	R_{ac}	a_c	R_{ac}	a_c
0	1707.8	3.13	1707.7617	3.1163	1707.7617	3.1163	1707.7617	3.1163
10	1945.9	3.25	1945.7457	3.2653	1945.7456	3.2652	1945.7456	3.2652
50	2802.1	3.68	2802.0058	3.6792	2802.0058	3.6792	2802.0058	3.6792
100	3757.4	4.00	3757.2301	4.0120	3757.2301	4.0120	3757.2301	4.0120
200	5488.6	4.45	5488.5332	4.4458	5488.5332	4.4458	5488.5332	4.4458

Table 6 Comparison of our numerical and semi-analytical results given by CGLSM, GDQM and WGWRT, in the case of electrically conducting nanofluids , when $R_N = 0.1$, $L_e = 5000$, $N_b = 10^{-6}$ and $N_t = 10^{-6}$.

Q	Present Numerical and Semi-Analytical Results					
	CGLSM ($N = 28$)		GDQM ($N = 28$)		WGWRT ($N = 15$)	
	R_{ac}	a_c	R_{ac}	a_c	R_{ac}	a_c
0	846.86043	2.43637	846.86042	2.43637	846.86043	2.43638
100	3091.08440	3.83811	3091.08440	3.83812	3091.08440	3.83812
200	4860.63528	4.33833	4860.63528	4.33834	4860.63528	4.33833
300	6485.38722	4.66476	6485.38722	4.66473	6485.38722	4.66474
400	8029.93455	4.91140	8029.93455	4.91143	8029.93455	4.91142
500	9521.32407	5.11151	9521.32407	5.11151	9521.32407	5.11151
600	10974.01001	5.28079	10974.01001	5.28078	10974.01001	5.28078
700	12396.81589	5.42804	12396.81589	5.42804	12396.81589	5.42805
800	13795.60743	5.55875	13795.60743	5.55874	13795.60744	5.55875
900	15174.52413	5.67649	15174.52414	5.67648	15174.52414	5.67649
1000	16536.61956	5.78378	16536.61956	5.78377	16536.61958	5.78379

5. CLOSING REMARKS

A generalized nanofluid model has been developed in this investigation for alumina-water nanofluids, in order to examine the thermo-magneto-hydrodynamic stability in a thin nanofluid layer. Under the Oberbeck-Boussinesq approximation, the governing partial differential equations (PDEs) were derived formally based on Buongiorno's, Chon's and Corcione's nanofluid models. By applying the linear stability theory and the normal mode analysis method, the resulting dimensionless PDEs are converted into a set of dimensionless ordinary differential equations (ODEs). These ODEs together with the boundary conditions constitute an eigenvalue problem, which has been solved numerically using Chebyshev-Gauss-Lobatto Spectral Method (CGLSM) and Generalized Differential Quadrature Method (GDQM). Moreover, our numerical findings have been validated and discussed in detail via tabular and graphical illustrations, in the case of isothermal impermeable plates with no-slip and zero nanoparticles mass flux conditions. The important findings derived from the present analysis are summarized as follows:

- The numerical results given by CGLSM and GDQM are presented in this paper with an absolute accuracy of the order of 10^{-6} and validated with the results of other powerful methods like VM, WGWRT and RKFM.
- Due to the zero nanoparticles mass flux condition, the volumetric fraction of alumina nanoparticles Al_2O_3 is controlled passively by the resulting temperature gradient on the impermeable plates.
- Based on the results of the proposed nanofluid model, it is found that the basic dimensional volumetric fraction of alumina nanoparticles Al_2O_3 at the hot plate ϕ_h^* and cold plate ϕ_c^* verify the two criterions $\phi_h^* + \phi_c^* = 2\phi_0$ and $\phi_c^* > \phi_h^*$.
- The thermo-magneto-hydrodynamic stability of alumina-water nanofluids increases with the increase in the magnetic Chandrasekhar number Q, while it decreases significantly with the increase in the volumetric fraction ϕ_0 and the diameter d_{np} of alumina nanoparticles.
- The presence of an applied transverse magnetic field has a stabilizing effect on the onset of magneto-convection in alumina-water nanofluids.
- Brownian motion and thermophoresis slip mechanisms have a destabilizing impact on the onset of magneto-convection in alumina-water nanofluids.
- The electrically conducting fluids are generally more stable than their corresponding nanofluids.
- An increase in the magnetic Chandrasekhar number Q leads to a reduction in the critical size of convection cells L_c , while the volumetric fraction ϕ_0 and the diameter d_{np} of alumina nanoparticles Al_2O_3 increase the critical size of convection cells L_c.

ACKNOWLEDGEMENTS

The authors wish to express their sincere gratitude to the peer reviewers, for their helpful suggestions and valuable comments, which have improved the paper appreciably.

REFERENCES

Akbarzadeh, P. (2018). "The Onset of MHD Nanofluid Convection Between a Porous Layer in the Presence of Purely Internal Heat Source and Chemical Reaction." *Journal of Thermal Analysis and Calorimetry*, **131**, 2657-2672.
https://doi.org/10.1007/s10973-017-6710-9

Alsabery, A. I., Sheremet, M. A., Chamkha, A. J., and Hashim, I. (2018). "Conjugate Natural Convection of Al2O3–Water Nanofluid in a Square Cavity with a Concentric Solid Insert Using Buongiorno's Two-Phase Model." *International Journal of Mechanical Sciences*, **136**, 200-219.
https://doi.org/10.1016/j.ijmecsci.2017.12.025

Amanulla, C. H., Wakif, A., Boulahia, Z., Suryanarayana Reddy, M., and Nagendra, N. (2018). "Numerical Investigations on Magnetic Field Modeling for Carreau Non-Newtonian Fluid Flow Past an Isothermal Sphere." *Journal of the Brazilian Society of Mechanical Sciences and Engineering*, **40:462**, 1-15.
https://doi.org/10.1007/s40430-018-1385-0

Angayarkanni, S. A., and Philip, J. (2015). "Review on Thermal Properties of Nanofluids : Recent Developments." *Advances in Colloid and Interface Science*, **225**, 146-176.
https://doi.org/10.1016/j.cis.2015.08.014

Animasaun, I. L. (2016) "47nm alumina–water nanofluid flow within boundary layer formed on upper horizontal surface of paraboloid of revolution in the presence of quartic autocatalysis chemical reaction." *Alexandria Engineering Journal*, **55**, 2375 - 2389
http://dx.doi.org/10.1016/j.aej.2016.04.030

Animasaun, I. L., Koriko, O. K., Adegbie, K. S., Babatunde, H. A., Ibraheem, R. O., Sandeep, N., and Mahanthesh, B. (2018). "Comparative analysis between 36 nm and 47 nm alumina–water nanofluid flows in the presence of Hall effect." *Journal of Thermal Analysis and Calorimetry*., 1-14.
http://dx.doi.org/10.1007/s10973-018-7379-4

Animasaun, I. L. and Pop I. (2017) "Numerical exploration of a non-Newtonian Carreau fluid flow driven by catalytic surface reactions on an upper horizontal surface of a paraboloid of revolution, buoyancy and stretching at the free stream." *Alexandria Engineering Journal*, **56**, 647 - 658.
https://doi.org/ 10.1016/j.aej.2017.07.005

Astanina, M. S., Abu-Nada, E., and Sheremet, M. A. (2018). "Combined Effects of Thermophoresis, Brownian Motion, and Nanofluid Variable Properties on CuO-Water Nanofluid Natural Convection in a Partially Heated Square Cavity." *Journal of Heat Transfer*, **140**, 1-12.
https://doi.org/10.1115/1.4039217

Boulahia, Z., Wakif, A., and Sehaqui, R. (2016). "Numerical Study of Mixed Convection of the Nanofluids in Two-Sided Lid-Driven Square Cavity with a Pair of Triangular Heating Cylinders." *Journal of Engineering*, **2016**(Article ID 8962091), 1-8.
https://doi.org/10.1155/2016/8962091

Boulahia, Z., Wakif, A., Chamkha, A. J., and Sehaqui, R. (2017a). "Numerical Study of Natural and Mixed Convection in a Square Cavity Filled by a Cu-Water Nanofluid with Circular Heating and Cooling Cylinders." *Mechanics and Industry*, **18**, 1-21.
https://doi.org/10.1051/meca/2017021

Boulahia, Z., Wakif, A., and Sehaqui, R. (2017b). "Finite Volume Analysis of Free Convection Heat Transfer in a Square Enclosure Filled by a Cu-Water Nanofluid Containing Different Shapes of Heating Cylinder." *Journal of Nanofluids*, **6**, 761-768.
https://doi.org/10.1166/jon.2017.1363

Boulahia, Z., Wakif, A., and Sehaqui, R. (2017c). "Modeling of Free Convection Heat Transfer Utilizing Nanofluid Inside a Wavy Enclosure with a Pair of Hot and Cold Cylinders." *Frontiers in Heat and Mass Transfer (FHMT)*, **8**, 1-10.
https://doi.org/10.5098/hmt.8.14

Boulahia, Z., Wakif, A., and Sehaqui, R. (2017d). "Numerical Modeling of Natural Convection Heat Transfer in a Wavy Wall Enclosure Filled by a Cu - Water Nanofluid with a Square Cooler." *Journal of Nanofluids*, **6**, 324-333.
https://doi.org/10.1166/jon.2017.1315

Boulahia, Z., Wakif, A., and Sehaqui, R. (2018). "Heat Transfer and Cu-Water Nanofluid Flow in a Ventilated Cavity Having Central Cooling Cylinder and Heated from the Below Considering Three Different Outlet Port Locations." *Frontiers in Heat and Mass Transfer*, **11**, 1-10.
https://doi.org/10.5098/hmt.11.11

Buongiorno, J. (2006). "Convective Transport in Nanofluids." *Journal of Heat Transfer*, **128**, 240-250.
https://doi.org/10.1115/1.2150834

Buongiorno, J. et al . (2009). "A Benchmark Study on the Thermal Conductivity of Nanofluids." *Journal of Applied Physics*, **106**, 1–14.
https://doi.org/10.1063/1.3245330

Canuto, C., Hussaini, M. Y., Quarteroni, A. M., and Thomas Jr, A. (2012). *Spectral Methods in Fluid Dynamics*. Springer Science & Business Media.

Chandrasekhar, S. (1961). *Hydrodynamic and hydromagnetic stability*. Oxford University Press, Oxford.

Choi, S. U. S. (1995). "Enhancing Tthermal Conductivity of Fluids with Nanoparticles." *ASME - Publications - Fed*, **231**, 99-106.

Chon, C. H., Kihm, K. D., Lee, S. P., and Choi, S. U. S. (2005). "Empirical Correlation Finding the Role of Temperature and Particle Size for Nanofluid (Al2O3) Thermal Conductivity Enhancement." *Applied Physics Letters*, **87**, 1-3.
https://doi.org/10.1063/1.2093936

Corcione, M. (2011). "Empirical Correlating Equations for Predicting the Effective Thermal Conductivity and Dynamic Viscosity of Nanofluids." *Energy Conversion and Management*, **52**, 789-793.
https://doi.org/10.1016/j.enconman.2010.06.072

Fidanoglu, M., Baskaya, E., Komurgoz, G., and Ozkol, I. (2014). "Application of Differential Quadrature Method and Evolutionary Algorithm to MHD Fully Developed Flow of a Couple-Stress Fluid in a Vertical Channel With Viscous Dissipation and Oscillating Wall Temperature." *ASME 2014 12th Biennial Conference on Engineering Systems Design and Analysis*, 1-9.
https://doi.org/10.1115/ESDA2014-20137

Garnett, J. C. M. (1905). "Colours in Metal Glasses, in Metallic Films and in Metallic Solutions." *Proc. R. Soc. Lond. A*, **76**, 370-373.

Garoosi, F., and Talebi, F. (2017). "Numerical Simulation of Conjugate Conduction and Natural Convection Heat Transfer of Nanofluid Inside a Square Enclosure Containing a Conductive Partition and Several Disconnected Conducting Solid Blocks Using the Buongiorno's Two Phase Model." *Powder Technology*, **317**, 48-71.
https://doi.org/10.1016/j.powtec.2017.04.042

Koriko, O. K., Animasaun, I. L., Mahanthesh, B., Saleem, S., Sarojamma, G., and Sivaraj, R. (2018). "Heat Transfer in the Flow of Blood-gold Carreau Nanofluid Induced by Partial Slip and Buoyancy." *Heat Transfer-Asian Research*, **47**, 806-823.
https://doi.org/10.1002/htj.21342

Makinde, O. D. , and Animasaun, I. L. (2016a). "Bioconvection in MHD nanofluid flow with nonlinear thermal radiation and quartic autocatalysis chemical reaction past an upper surface of a paraboloid of revolution." *International Journal of Thermal Sciences*, **109**, 159 - 171.
https://doi.org/10.1016/j.ijthermalsci.2016.06.003

Makinde, O. D. , and Animasaun, I. L. (2016b). "Thermophoresis and Brownian motion effects on MHD bioconvection of nanofluid with nonlinear thermal radiation and quartic chemical reaction past an upper horizontal surface of a paraboloid of revolution." *Journal of Molecular Liquids*, **221**, 733 - 743.

Makinde, O.D., Omojola, M.T., Mahanthesh, B., Alao, F.I., Adegbie, K.S., Animasaun, I. L., Wakif , A., Sivaraj, R., and Tshehla, M.S. (2018). "Significance of Buoyancy, Velocity Index and Thickness of an Upper Horizontal Surface of a Paraboloid of Revolution: The Case of Non-Newtonian Carreau Fluid." *Defect and Diffusion Forum*, **387**, 550-561. https://doi.org/10.4028/www.scientific.net/DDF.387.550

Maxwell, J.C.A., (1873). Treatise on electricity and magnetism. 2nd ed. Oxford, UK: Clarendon Press. https://doi.org/10.1016/j.molliq.2016.06.047

McNab, G. S., and Meisen, A. (1973). "Thermophoresis in Liquids." *Journal of Colloid and Interface Science*, **44**, 339-346.

Mehmood, K., Hussain, S., and Sagheer, M. (2017). "Mixed Convection in Alumina-Water Nanofluid Filled Lid-Driven Square Cavity with an Isothermally Heated Square Blockage Inside with Magnetic Field Effect : Introduction." *International Journal of Heat and Mass Transfer*, **109**, 397-409. https://doi.org/10.1016/j.ijheatmasstransfer.2017.01.117

Naddaf, A., and Heris, S. Z. (2018). "Experimental Study on Thermal Conductivity and Electrical Conductivity of Diesel Oil-Based Nanofluids of Graphene Nanoplatelets and Carbon Nanotubes." *International Communications in Heat and Mass Transfer*, **95**, 116-122. https://doi.org/10.1016/j.icheatmasstransfer.2018.05.004

Nguyen, C. T., Desgranges, F., Roy, G., Galanis, N., Mare, T., Boucher, S., and Minsta, H. A. (2007). "Temperature and Particle-Size Dependent Viscosity Data for Water Based Nanofluids- Hysteresis Phenomenon." *Int. J. Heat Fluid Flow*, **28**, 1492-1506. https://doi.org/10.1016/j.ijheatfluidflow.2007.02.004

Nield, D. A., and Kuznetsov, A. V. (2014a). "The Onset of Convection in a Horizontal Nanofluid Layer of Finite Depth : A Revised Model." *International Journal of Heat and Mass Transfer*, **77**, 915-918. https://doi.org/10.1016/j.ijheatmasstransfer.2014.06.020

Nield, D. A., and Kuznetsov, A. V. (2014b). "Thermal Instability in a Porous Medium Layer Saturated by a Nanofluid: A Revised Model." *International Journal of Heat and Mass Transfer*, **68**, 211-214. https://doi.org/10.1016/j.ijheatmasstransfer.2013.09.026

Pandey, A. K., and Kumar, M. (2016). "Effect of Viscous Dissipation and Suction/Injection on MHD Nanofluid Flow Over a Wedge with Porous Medium and Slip." *Alexandria Engineering Journal*, **55**, 3115-3123. https://doi.org/10.1016/j.aej.2016.08.018

Pandey, A. K., and Kumar, M. (2017a). "Boundary Layer Flow and Heat Transfer Analysis on Cu-Water Nanofluid Flow Over a Stretching Cylinder with Slip." *Alexandria Engineering Journal*, **56**, 671-677. https://doi.org/10.1016/j.aej.2017.01.017

Pandey, A. K., and Kumar, M. (2017b). "Chemical Reaction and Thermal Radiation Effects on Boundary Layer Flow of Nanofluid Over a Wedge with Viscous and Ohmic Dissipation." *St. Petersburg Polytechnical University Journal: Physics and Mathematics*, **3**, 322-332. https://doi.org/https://doi.org/10.1016/j.spjpm.2017.10.008

Pandey, A. K., and Kumar, M. (2017c). "Natural Convection and Thermal Radiation Influence on Nanofluid Flow Over a Stretching Cylinder in a Porous Medium with Viscous Dissipation." *Alexandria Engineering Journal*, **56**, 55-62. https://doi.org/10.1016/j.aej.2016.08.035

Qasim, M., Ali, Z., Wakif, A., and Boulahia, Z. (2018). "Numerical Simulation of MHD Peristaltic Flow with Variable Electrical Conductivity and Joule Dissipation Using Generalized Differential Quadrature Method." *Communications in Theoretical Physics*, ***In Press***.

Rana, P., Khurana, M., and Srivastava, S. (2017). "Linear Stability Analysis on the Onset of MHD Non-Newtonian Viscoelastic Rotating Nanofluid Layer with Heat Generation." In *AIP Conference Proceedings* (Vol. 1897, pp. 1-8). AIP Publishing. https://doi.org/10.1063/1.5008709

Schenck, J. F. (1996). "The Role of Magnetic Susceptibility in Magnetic Resonance Imaging: MRI Magnetic Compatibility of the First and Second Kinds." *Medical Physics*, **23**, 815-850. https://doi.org/10.1118/1.597854

Shah, N. A., Animasaun, I. L., Ibraheem, R. O., Babatunde, H. A., Sandeep, N., and Pop, I. (2018). "Scrutinization of the Effects of Grashof Number on the Flow of Different Fluids Driven by Convection over Various Surfaces." *Journal of Molecular Liquids*, **249**, 980-990. https://doi.org/10.1016/j.molliq.2017.11.042

Shu, C. (2012). *Differential quadrature and its application in engineering*. Springer Science & Business Media.

Sihvola, A. H., and Lindell, I. V. (1992). "Effective Permeability of Mixtures." *Progr. Electromagn. Res.*, **6**, 153-180.

Trefethen, L. N. (2000). *Spectral Methods in MATLAB*. SIAM.

Wakif, A., Boulahia, Z., Ali, F., Eid, M. R., and Sehaqui, R. (2018a). "Numerical Analysis of the Unsteady Natural Convection MHD Couette Nanofluid Flow in the Presence of Thermal Radiation Using Single and Two-Phase Nanofluid Models for Cu–Water Nanofluids." *International Journal of Applied and Computational Mathematics*, **4 : 81**, 1-27. https://doi.org/10.1007/s40819-018-0513-y

Wakif, A., Boulahia, Z., and Sehaqui, R. (2017a). "Numerical Analysis of the Onset of Longitudinal Convective Rolls in a Porous Medium Saturated by an Electrically Conducting Nanofluid in the Presence of an External Magnetic Field." *Results in Physics*, **7**, 2134-2152. https://doi.org/10.1016/j.rinp.2017.06.003

Wakif, A., Boulahia, Z., Mishra, S. R., Rashidi, M. M., and Sehaqui, R. (2018b). "Influence of a Uniform Transverse Magnetic Field on the Thermo - Hydrodynamic Stability in Water-Based Nanofluids with Metallic Nanoparticles Using the Generalized Buongiorno's Mathematical Model." *The European Physical Journal Plus*, **133:181**, 1-16. https://doi.org/10.1140/epjp/i2018-12037-7

Wakif, A., Boulahia, Z., and Sehaqui, R. (2018c). "A Semi-Analytical Analysis of Electro-Thermo-Hydrodynamic Stability in Dielectric Nanofluids Using Buongiorno's Mathematical Model Together with More Realistic Boundary Conditions." *Results in Physics*, **9**, 1438-1454. https://doi.org/10.1016/j.rinp.2018.01.066

Wakif, A., Boulahia, Z., and Sehaqui, R. (2017b). "Numerical Study of the Onset of Convection in a Newtonian Nanofluid Layer with Spatially Uniform and Non Uniform Internal Heating." *Journal of Nanofluids*, **6**, 136-148. https://doi.org/10.1166/jon.2017.1293

Wakif, A., Boulahia, Z., and Sehaqui, R. (2016). "Analytical and Numerical Study of the Onset of Electroconvection in a Dielectric Nanofluid Saturated a Rotating Darcy Porous Medium." *International Journal of Advanced Computer Science and Applications*, **7**, 299-311. https://doi.org/10.14569/ijacsa.2016.070841

Żyła, G., and Fal, J. (2017). "Viscosity, Thermal and Electrical Conductivity of Silicon Dioxide-Ethylene Glycol Transparent Nanofluids: An Experimental Studies." *Thermochimica Acta*, **650**, 106-113. https://doi.org/10.1016/j.tca.2017.02.001

Żyła, G., Vallejo, J. P., Fal, J., and Lugo, L. (2018). "Nanodiamonds-Ethylene Glycol Nanofluids: Experimental Investigation of Fundamental Physical Properties." *International Journal of Heat and Mass Transfer*, **121**, 1201-1213. https://doi.org/10.1016/j.ijheatmasstransfer.2018.01.073